Pontifícia Universidade Católica do Rio Grande do Sul
Faculdade de Biociências
Programa de Pós-Graduação em Biologia Celular e Molecular

A enzima 2-*trans*-enoil-ACP (CoA) redutase de *Mycobacterium tuberculosis*: estudos de ligação e inibição por um complexo inorgânico derivado da isoniazida

Dissertação apresentada ao Programa de Pós-Graduação em Biologia Celular e Molecular como requisito para a obtenção do grau de Mestre.

Autor
Igor Bordin Vasconcelos

Orientador
Luiz Augusto Basso

Co-orientador
Diógenes Santiago Santos

Porto Alegre, RS
Novembro/2007

Dedico este trabalho a minha mãe e meu pai, Maria Verônica e Paulo Willian, a minha irmã, Milene, e a minha namorada, Josiane, pelo apoio e incentivo de todos.

Agradecimentos

Aos meus orientadores, Prof. Luiz Augusto Basso e Diógenes Santiago Santos, pela oportunidade de desenvolver este trabalho em seu grupo de pesquisa, pelos ensinamentos práticos e teóricos durante a realização do mesmo e pela confiança em mim depositada para a realização do projeto.

A todos os colegas e colaboradores do Centro de Pesquisas em Biologia Molecular e Funcional e da 4G.

Ao grupo de pesquisas do Departamento de Química Orgânica e Inorgânica da Universidade Federal do Ceará, sob a coordenação do Prof. Ícaro de Sousa Moreira.

Ao Programa de Pós-Graduação em Biologia Celular e Molecular da PUCRS.

Ao Laboratório Americano de Farmacoterapia S.A. (FARMASA) pela bolsa de estudos para realizar o curso de Mestrado.

Índice Geral

Índice de Tabelas

Índice de Figuras

Resumo

A tuberculose (TB) continua sendo a principal causa de mortalidade devido a um único patógeno bacteriano, *Mycobacterium tuberculosis*. A reemergência da tuberculose como uma ameaça potencial à saúde pública, a alta suscetibilidade de pessoas infectadas com o vírus da imunodeficiência humana à doença, a proliferação de cepas resistentes a múltiplas drogas (MDR-TB) e, mais recentemente, de cepas extensivamente resistentes às drogas (XDR-TB) criaram a necessidade do desenvolvimento de novos agentes antimicobacterianos. Existe uma necessidade contínua de inovação em propor novas estruturas para o desenvolvimento de agentes quimioterápicos para o controle da TB. Os ácidos micólicos, característicos de micobactérias, são ácidos graxos α-alquil, β-hidróxi de alto peso molecular que aparecem, principalmente, como ésteres ligados ao envelope micobacteriano. A isoniazida (INH) é o agente quimioterápico mais prescrito para a TB ativa e para a profilaxia e necessita de ativação pela atividade de catalase-peroxidase da KatG. O produto do gene estrutural *M.tuberculosis inhA* (InhA) demonstrou ser o alvo primário da INH. A InhA foi identificada como uma enoil-ACP redutase dependente de NADH, possuindo especificidade por enoil tioésteres de cadeia longa. InhA é um membro do sistema de biossíntese de ácidos graxos micobacterianos do tipo II que elonga ácidos graxos acilados, precursores dos ácidos micólicos. O foco principal de nossa contribuição são dados descrevendo o modo de ação de um complexo inorgânico, pentaciano (isoniazida) ferrato II que não necessita de ativação pela KatG. Ademais é um inibidor do tipo ligação lenta da enoil redutase WT e resistente à INH de *M.tuberculosis*. Este complexo inorgânico representa uma nova classe de compostos líderes para o desenvolvimento de agentes antituberculose objetivando a inibição de um alvo validado. Nós também descrevemos os avanços recentes na busca por complexos inorgânicos com atividade antituberculose.

Palavras-chave: tuberculose, ácidos micólicos, InhA, isoniazida, inibição ligação lenta, complexo inorgânico, resistência a drogas.

Abstract

Tuberculosis (TB) remains the leading cause of mortality due to a single bacterial pathogen, *Mycobacterium tuberculosis*. The reemergence of tuberculosis as a potential public health threat, the high susceptibility of human immunodeficiency virus-infected persons to the disease, the proliferation of multi-drug-resistant strains (MDR-TB) and, more recently, of extensively drug resistant isolates (XDR-TB) have created a need for the development of new antimycobacterial agents. There is an ongoing need for innovation in proposing new structural scaffolds for chemotherapeutic agent development to control TB. Mycolic acids, the hallmark of mycobacteria, are high-molecular-weight α-alkyl, β-hidroxy fatty acids, which appear mostly as bound esters in the mycobacterial envelope. Isoniazid (INH) is the most prescribed chemotherapeutic agent for active TB and prophylaxis and requires activation by the catalase-peroxidase activity of KatG. The product of the *M.tuberculosis inhA* structural gene (InhA) has been shown to be the primary target for INH. InhA was identified as an NADH-dependent enoyl-ACP reductase specific for long chain enoyl thioesters. InhA is a member of the mycobacterial Type II fatty acid biosynthesis system, which elongates acyl fatty acid precursors of mycolic acids. The main focus of our contribution is on data describing the mode of action of an inorganic complex, pentacyano (isoniazid) ferrateII that requires no KatG-activation and is an *in vitro* slow-onset inhibitor of WT and INH-resistant *M.tuberculosis* enoyl reductases. This inorganic complex represents a new class of lead compounds to the development of anti-tubercular agents aiming the inhibition of a validated target. We also describe the recent developments in the search for inorganic complexes with anti-tubercular activity.

1. Apresentação da dissertação

A presente dissertação de mestrado foi desenvolvida no período de agosto de 2006 a setembro de 2007, sob a orientação dos professores Luiz Augusto Basso e Diógenes Santiago Santos. Este trabalho foi realizado no Centro de Pesquisas em Biologia Molecular e Funcional (CPBMF), localizado no TecnoPUC – PUCRS.

As seções de introdução, resultados e discussão serão apresentadas na forma de um artigo (seção 2) que reporta os resultados experimentais mais relevantes obtidos durante o período de mestrado. O artigo é intitulado “The Mode of Inhibition of *Mycobacterium tuberculosis* Wild-Type and Isoniazid-Resistant 2-*Trans*-Enoyl-ACP(CoA) reductase enzymes by an inorganic complex” e foi aceito para publicação na revista Anti-Infective Agents in Medicinal Chemistry em abril de 2007. Até o ano de 2005, esta revista era publicada como uma divisão do periódico Current Medicinal Chemistry, classificada como Qualis A pela Capes, possuindo um fator de impacto de 4,9 (ISI Web of Knowledge - 2005), sendo que, atualmente, ela é publicada independentemente.

Na parte introdutória do artigo, são abordados a epidemiologia e quimioterapia da tuberculose, a biossíntese de ácidos micólicos em *M.tuberculosis* salientando o papel da enzima 2-*trans*-enoil-ACP(CoA) redutase (InhA) nesta rota metabólica e também sua importância como o principal alvo da droga utilizada no tratamento da tuberculose, a hidrazida do ácido isonicotínico (isoniazida). Além disso, são descritos os mecanismos de ação e resistência à isoniazida em *M.tuberculosis* e os esforços recentes para o desenvolvimento de novos inibidores da enzima enoil redutase de *M.tuberculosis* através do uso de complexos inorgânicos derivados da estrutura da isoniazida.

Posteriormente, são apresentados e discutidos dados que demonstram o mecanismo de ligação e inibição da enzima InhA espécie selvagem e mutantes resistentes à isoniazida pelo composto pentaciano(isoniazida)ferratoII como sendo do tipo “ligação lenta”. No mecanismo de inibição, inicialmente, ocorre a rápida formação de um complexo binário entre a enzima e o inibidor EI, o qual sofre uma isomerização unimolecular lenta para um estado EI^*, onde o inibidor encontra-se mais fortemente ligado à enzima. Os resultados deste artigo demonstram que este complexo inorgânico pode representar uma nova classe de compostos líderes para o desenvolvimento de agentes anti-tuberculose visando a inibição de um alvo validado.

Na seção 3, “considerações finais”, será feita uma discussão e integração dos resultados apresentados no artigo com os objetivos da dissertação e desta pesquisa em geral que visa o desenvolvimento de novos agentes quimioterápicos para o tratamento da tuberculose.

Por fim, na seção 5, “anexos”, são apresentados todos os artigos publicados durante o período de mestrado e iniciação científica que resultaram de atividades realizadas pelo presente autor em outros projetos.

2. The mode of inhibition of *Mycobacterium tuberculosis* wild-type and isoniazid-resistant 2-*trans*-enoyl-ACP(CoA) reductase enzymes by an inorganic complex (Artigo aceito para publicação na revista "Anti-Infective Agents in Medicinal Chemistry" em abril de 2007)

The Mode of Inhibition of *Mycobacterium tuberculosis* Wild-Type and Isoniazid-Resistant 2-*Trans*-Enoyl-ACP(CoA) Reductase Enzymes by An Inorganic Complex

I.B. Vasconcelos[a], E. Meyer[b], F.A.M. Sales[b], I.S. Moreira[b], L.A. Basso[a,*] and D.S. Santos[a,*]

[a]*Pontifícia Universidade Católica do Rio Grande do Sul, Centro de Pesquisas em Biologia Molecular e Funcional, Porto Alegre, RS, Brasil;* [b]*Departamento de Química Orgânica e Inorgânica, Universidade Federal do Ceará, Fortaleza, Brazil*

Abstract: Tuberculosis (TB) remains the leading cause of mortality due to a single bacterial pathogen, *Mycobacterium tuberculosis*. The reemergence of tuberculosis as a potential public health threat, the high susceptibility of human immunodeficiency virus-infected persons to the disease, the proliferation of multi-drug-resistant strains (MDR-TB) and, more recently, of extensively drug resistant isolates (XDR-TB) have created a need for the development of new antimycobacterial agents. There is an ongoing need for innovation in proposing new structural scaffolds for chemotherapeutic agent development to control TB. Mycolic acids, the hallmark of mycobacteria, are high-molecular-weight α-alkyl, β-hidroxy fatty acids, which appear mostly as bound esters in the mycobacterial envelope. Isoniazid (INH) is the most prescribed chemotherapeutic agent for active TB and prophylaxis and requires activation by the catalase-peroxidase activity of KatG. The product of the *M.tuberculosis inhA* structural gene (InhA) has been shown to be the primary target for INH. InhA was identified as an NADH-dependent enoyl-ACP reductase specific for long chain enoyl thioesters. InhA is a member of the mycobacterial Type II fatty acid biosynthesis system, which elongates acyl fatty acid precursors of mycolic acids. The main focus of our contribution is on data describing the mode of action of an inorganic complex, pentacyano (isoniazid) ferrateII that requires no KatG-activation and is an *in vitro* slow-onset inhibitor of WT and INH-resistant *M.tuberculosis* enoyl reductases. This inorganic complex represents a new class of lead compounds to the development of anti-tubercular agents aiming the inhibition of a validated target. We also describe the recent developments in the search for inorganic complexes with anti-tubercular activity.

Keywords: Tuberculosis, mycolic acids, InhA, isoniazid, slow-onset inhibition, inorganic complex, drug resistance.

1. INTRODUCTION

Tuberculosis (TB) is the world leading cause of mortality owing to an infectious bacterial agent, *Mycobacterium tuberculosis*. Historian established the existence of endemic TB from Egyptian mummies dating from 2000 to 4000 B.C. [1]. Modern techniques of molecular genetics and the sequencing of the genome of several strains of *M.tuberculosis* led to the conclusion that an early progenitor of *M.tuberculosis* was present in East Africa as early as 3 million years ago, and suggest that it may have infected early hominids at that time [2]. TB was responsible for 20% of all deaths in London in 1651, and the disease may have accounted for a third of all deaths in Paris in the 19th century. As Europeans colonized the Americas and sub-Saharan Africa, the disease was passed to susceptible populations and spread worldwide [3]. The interruption of centuries of decline in case rates of TB occurred, in most cases, in the late 1980s and involved the US and some European countries due to increased poverty in urban settings and the immigration from TB high-burden countries [4]. Thus, no sustainable control of TB epidemics can be reached in any country without properly addressing the global epidemic. According to the 2006 Global TB Control Report of the WHO, it is estimated that 9 million new TB cases occurred worldwide in the year 2004, with approximately 2 million deaths in the same year, and more than 80% of all TB patients live in sub-Saharan Africa and Asia [5]. In addition, the number of TB cases was stable or falling in 5 of 6 WHO regions, but growing in Africa where the TB epidemic is still driven by the spread of human immunodeficiency virus (HIV). Approximately 1/3 of the world's population is believed to harbor latent TB, based on tuberculin skin test surveys [6]. People with latent TB infection are at higher risk of progression to active disease if coinfected with HIV as compared to HIV-negative persons [7], and approximately 12% of total deaths from TB were attributable to coinfection with HIV [8]. It has been estimated that in the year 2003 the median prevalence of resistance to any of the first-line drugs, most commonly streptomycin or isoniazid (INH) was 10.7% in patients that had not been previously treated [9]. According to the 2006 WHO Report, based on a combination of surveys and estimates, approximately 460 000 (17%) of the world's new cases of TB in 2004 were multidrug-resistant tuberculosis (MDR-TB), defined as resistant to at least isoniazid and rifampicin. More recently, extensively drug-resistant strains (XDR-TB), defined as resistant to at least three of the six classes of available second-line drugs in addition to MDR-

*Address correspondence to these authors at the Pontifícia Universidade Católica do Rio Grande do Sul, Centro de Pesquisas em Biologia Molecular e Funcional, Porto Alegre, RS, Brasil; Tel:/Fax: +55 51 3320 3629; E-mails: diogenes@pucrs; luiz.basso@pucrs.br

1871-5214/08 $55.00+.00

TB, have been shown to have a wide geographic distribution [10]. XDR is a form of TB which leaves patients without treatment options that meet international standards, resulting in high treatment failure and is a serious threat to TB control wherever it emerges. In USA, Republic of Korea and Latvia, population-based studies showed that 4%, 15% and 19% respectively, of MDR-TB cases were XDR-TB. The main factors influencing the emergence of drug-resistant strains are inappropriate treatment regimens or patients failure to comply with the therapy, particularly when their symptoms subside as the drugs exert their effect, or when the side effects become unbearable [11]. Hence more effective and less toxic anti-tubercular agents are urgently needed to shorten the duration of current treatment, to improve the treatment of MDR-TB and XDR-TB, and to provide effective treatment of latent tuberculosis infection.

2. CHEMOTERAPY

Corpora Non Agunt Nisi Fixata (Paul Ehrlich, 1909)

In the turn of the twentieth century, Paul Ehrlich coined a phrase that became the basis of modern pharmacology and chemotherapy. Translated into a more contemporary concept, a drug is efficacious only as long as it is bound to its physiological target(s) and modulating or blocking its action. The modern approach to the development of new chemical entities against complex diseases, especially the neglected ones such as tuberculosis and malaria, is based on the use of defined molecular targets. The search for chemical entities against TB was made possible after 1882, when Robert Koch identified its causative agent, an acid-fast bacterium, *Mycobacterium tuberculosis*, which is a rod-shaped obligate aerobe, that survives best in an environment with a pO_2 of 100 to 140 mm Hg, 5% CO_2 and a physiologic pH of 7.4 [12]. The disease is spread from person to person almost exclusively by small-particle aerosols of sufficiently small size (1-5μm in diameter that may contain from 1 to 10 tubercle bacilli) so that they are inhaled into the alveolar space, where they are deposited and the organism begins to replicate. Tubercle bacilli divide slowly with a doubling time of approximately 24 hours [13]. This slow doubling time increases the length of time required for chemotherapy and makes drug susceptibility determinations time-consuming. *M.tuberculosis* is a highly successful pathogen. Under normal circumstances, the infection is held in check by the immune system of the host and, in ~90% of infected individuals, the infection does not give rise to the disease [14]. The ability of *M. tuberculosis* to persist in the host tissues makes drugs that are rapidly bactericidal *in vitro* require prolonged administration to achieve comparable effects[15].

The discovery of the antibacterial and antitubercular properties of streptomycin in 1944 [16], and both isoniazid and pyrazinamide in 1952 [17-18] led to effective chemotherapies that decreased TB mortality rate worldwide. The later introduction of ethionamide, rifampicin, ethambutol and ciprofloxacin to the arsenal used to treat TB seemed to provide an adequate number of effective antimicrobial agents. To obtain success in the treatment of TB, chemotherapy must include early bactericidal action against rapidly growing organisms, which includes the first-line drugs isoniazid, rifampicin, streptomycin and ethambutol, and subsequent sterilization of the semi-dormant bacilli, on which pyrazinamide is active [19]. The DOTS TB control strategy is a systematic approach to diagnosis, standardized treatment regimens, regular reviews of outcomes, assessment of effectiveness and modification of approaches when problems are identified [20]. The DOTS treatment regimen, which is adopted in most countries worldwide, is based on a four-drug regimen of isoniazid, rifampicin, pyrazinamide, and ethambutol or streptomycin for two months, followed by a combination of isoniazid and rifampicin for an additional four months. The bacteriostatic second-line drugs, which are more toxic and less effective, are reserved to the cases where drug resistance arises, and the treatment time is extended up to 2 years and at 100 times the cost of basic short-course chemotherapy regimens [21].

3. MYCOBACTERIAL CELL WALL

The cell envelope of *M .tuberculosis* is distinctive and is highly associated with its pathogenicity [22]. The mycobacterial envelope is composed of two segments, upper and lower. The cytoplasmic membrane is encapsulated by a rigid layer of peptidoglycan that is covalently attached to arabinogalactan, which, in turn, is bound to mycolic acids, the hallmark of mycobacteria (Fig. **1**) [23]. This covalently linked skeleton is often described as mycolyl-arabinogalactan-peptidoglycan complex (mAGP). This provides a layer on the outer part of the cell and protects the tubercle bacillus from noxious chemicals and the host's immune system.

The peptidoglican component of the cell wall is a polysaccharide chain composed of repeating N-acetyl-β-Dglucosaminyl-(1→4)-*N*-glycolylmuramic acid units cross-linked by L-alanyl-D-isoglutaminyl-*meso*-diaminopimelyl-D-alanine peptide chains linked to the lactoyl groups of muramic acids residues, being this type of peptidoglycan the most commonly found in bacteria. Mycobacterial peptidoglycan differs in two aspects: the muramic acid is *N*-acylated with glycolic acid rather than with the usual acetic acid found in all other bacteria, which may provide an enhanced rigidity of the mycobacterial peptidoglycan structure [24], and the peptide cross-links in the mycobacterial peptidoglycan include a proportion of bonds between two residues of *meso*-diaminopimelic acid (*meso*-DAP) instead of the more usual *meso*-DAP-D-alanine linkages.

The mycobacterial peptidoglycan structure is attached to arabinogalactan through a phosphodiester linkage between the C6 of about 10-12% of muramic acid residues and a disaccharide linker unit attached to the nonreducing terminus of the galactan. Arabinogalactan is a unique polysaccharide consisting of linear galactan chains composed of alternating 5- and 6-linked in the furanose form [β-D-Gal*f*-(1→5)-β-D-Gal*f*-(1→6)]$_n$ which, in turn, are attached through C5 of some of the 6-linked β-D-Gal*f* units to the extensively branched chains of D-Ara*f*-containing arabinan. The nonreducing termini of arabinan consist of a branched hexaarabinofuranosyl structure, of which about two-thirds are esterified to mycolic acids. Although the process of biosynthesis and maintenance of the cell wall structure is know to be the target of drugs used to kill replicating bacilli, such as isoniazid and ethionamide, it is also known that this structure

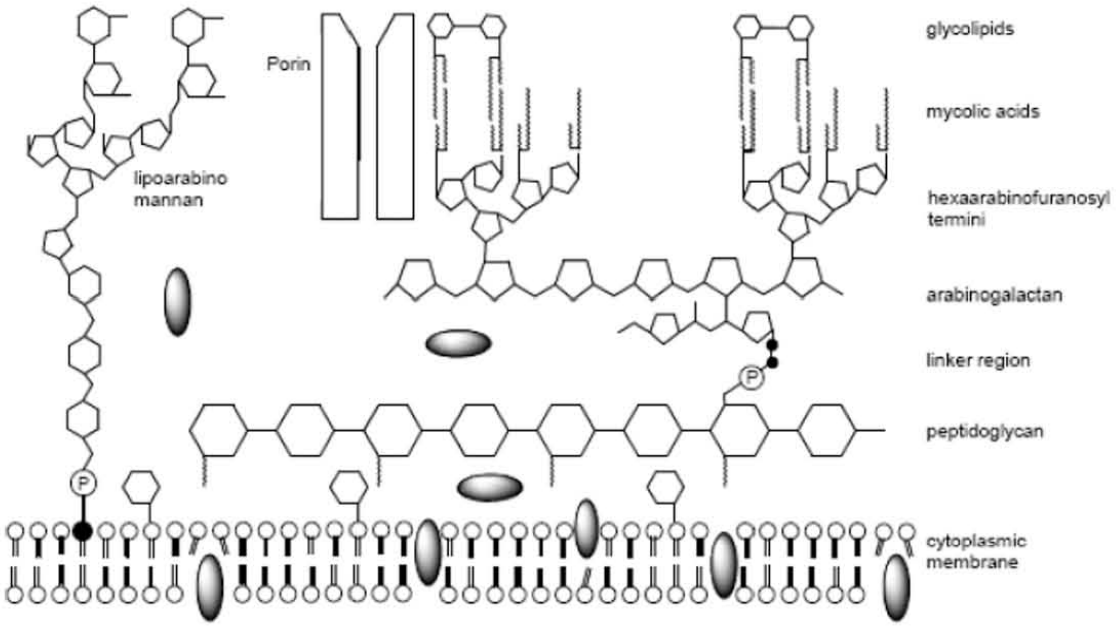

Fig. (1). Schematic representation of the mycobacterial cell wall. The cytoplasmic membrane is encapsulated by a layer of peptidoglycan. The peptidoglycan backbone is attached to arabinogalactan through an unusual disaccharide phosphate linker region. The arabinogalactan is a branched-chain polysaccharide consisting of a proximal galactose chain linked to a distal arabinose chain. The hexaarabinofuranosyl termini of arabinogalactan are esterified to mycolic acids. The mycolic acid chains are shown perpendicular to the cytoplasmic membrane with the exposed chains interacting with the mycolic chains of trehalose dimycolate.

is not static but is a dynamic polymer that adapts to intermittent phases of nonreplication, making the elements that participates of such modifications during latent phase a promising target for the development of new anti-TB agents [25].

3.1. Mycolic Acids: Structure and Biosynthesis

Mycolic acids have become one of the defining taxonomic characteristics of many species in genera such as *Mycobacterium*, *Corynebacterium*, *Dietzia*, *Nocardia*, and *Rhodococus*. Mycolic acids are high-molecular-weight α-alkyl, β-hydroxy fatty acids (Fig. **2**), appearing mostly as bound esters in tetramycolylpentaarabinosyl clusters in mycobacteria. In the pyrolytic cleavage of mycolic acids the intact fatty acid released is often referred to as the α branch because it occupies the alpha position with respect to the carboxylic acid group and the aldehyde released is referred to as the meroaldehyde, and the corresponding segment of the intact mycolate is thus referred to as the meromycolate branch. The meromycolate branch is functionalized at regular intervals by cyclopropyl, α-methyl ketone, or α-methyl methylethers groups [26, 27], and by unsaturations [28].

The main features that distinguish the mycolic acids from *M.tuberculosis* to those of other genera, like the ones above, are the following: (a) they are the largest, presenting C_{70} to C_{90} and α-branch of C_{20} to C_{26}; (b) their meromycolic acid moiety contains one or two groups, commonly double bonds or cyclopropane rings; (c) they may contain oxygen functions additional to the β-hydroxy group and methyl branches in the meromycolate chain. More recently, the structure of *Mt*Hma, also know as MmaA4, an enzyme essential for the biosynthesis of oxygenated mycolic acids, was solved in complex with S-adenosylmethionine at 2Å resolution, showing the important role played by modifications in the meromycolate chain by the introduction of a methyl branch [29]. The functional groups present in mycobacterial mycolic acids occur at two points in the meromycolate chain and are referred to as distal and proximal. Polar modifications are usually restricted to the distal position, including such functional groups as methyl ethers, ketones, esters, and epoxides. Nonpolar modifications occur at both the distal and the proximal positions and include *cis* or *trans* double bonds and *cis* or *trans* cyclopropanes. Deletion of the proximal cyclopropane ring of α-mycolate or deletion of the methoxy – and keto-mycolates leads to a significant attenuation of growth of mutants in a mouse model of infection, and deletion of keto-mycolates in *M. tuberculosis* restricted the growth in macrophages. Based on these observations, it can be concluded that mycolic acids are very important components of the pathogenic *M. tuberculosis*.

In the process of biosynthesis of mycolic acids, five general and distinct steps have been proposed to occur: (1) synthesis of 24- to 25-carbon straight chain saturated fatty acids to provide the α-alkyl branch; (2) synthesis of the meromycolic acid chain to provide the main carbon backbone; (3) introduction of other functional groups to the meromycolic acid chain; (4) the final Claisen-type condensation between the meromycolate chain and the α-branch, followed by reduction; and (5) mycolyltransferase processes to cellular lipids [30]. Fatty acid elongation occurs through repetitive cycles of condensation, β-keto reduction, dehydration, and enoyl reduction which are catalyzed by, respectively, β-ketoacyl synthase (KAS, condensing enzyme), β-ketoacyl reductase (KAR, MabA in *M.tuberculosis*), β-hydroxyacyl

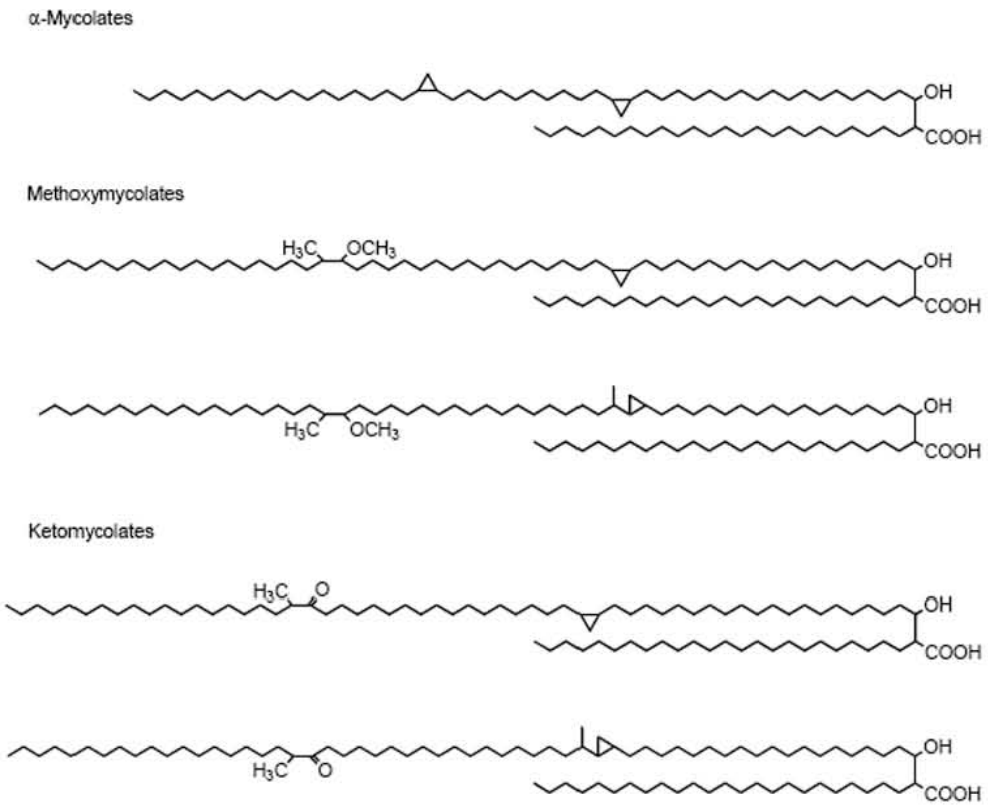

Fig. (2). The structures of mycolic acids identified in M. tuberculosis. α-mycolates: its meromycolate chain contains two cis-cyclopropane rings. Methoxymycolates: its meromycolate chain contains an α-methyl methylether moiety in the distal position and a cis-cyclopropane ring or an α-methyl trans-cyclopropane ring in the proximal position. Ketomycolates: its meromycolate chain contains an α-methyl ketone moiety in the distal position and proximal functionalities as in the methoxy series. The unsaturations are not shown here.

dehydrase (DE), and enoyl reductase (ENR, InhA in *M.tuberculosis)*. These chemical reactions are catalyzed by two types of fatty acid synthase systems (FAS). The FAS-I system is a multidomain polyprotein that encodes all the enzymes necessary for fatty acid synthesis in one large polypeptide and is generally present in most eukaryotes, except in plants [31]. FAS-II systems, which are present in bacteria and plants, catalyze the individual reactions by separate proteins which are encoded by unique genes. Unlike most organisms, mycobacteria have both FAS-I and FAS-II systems [32]. The mycobacterial FAS-I system is responsible not only for the synthesis of C_{16} and C_{18} fatty acids, the normal products of *de novo* synthesis, but also for elongation to produce C_{24} and C_{26} fatty acids [33]. The mycobacterial FAS-II is not capable of *de novo* synthesis, but instead elongates palmitoyl-ACP to fatty acids ranging from 24 to 56 carbons in length [34]. The mycobacterial FAS-I produces a bimodal ($C_{14:0}$-$C_{16:0}$ to $C_{24:0}$-$C_{26:0}$) distribution of acyl-CoA fatty acids. The mycobacterial FAS-I system would provide the shorter acyl-CoA fatty acid precursors ($C_{14:0}$-$C_{16:0}$) for condensation with malonyl-ACP by mtFabH enzyme activity whose products, in turn, would be elongated by the FAS-II system, yielding the long carbon chain of the meromycolate branch (50-60 carbons) of mycolic acids. The longer chain acyl-CoA products ($C_{24:0}$-$C_{26:0}$) of FAS-I would be excluded from chain elongation and remain available to be utilized, presumably in the CoA form, as substrates for formation of the α-alkyl branch (20-26 carbons) of mycolic acids. Although the proteins of the FAS-II system are codified by unique genes and their activities were characterized individually, it has been suggested that the components of FAS-II are interconnected by specific protein-protein interactions that are essential for mycobacterial survival. A combination of yeast two-hibrid and co-immunoprecipitation experiments showed that mtFabD interacts with each β-ketoacyl-synthase (KasA, KasB and mtFabH) and with the core of FAS-II (InhA and MabA) [35].

3.2. Isoniazid (INH) Mechanism of Action

Isoniazid (INH, isonicotinic acid hydrazide) was synthesized for the first time in 1912 by two Czech scientists [36], but its powerful antituberculosis activity was only discovered in 1951, and strains of *M.tuberculosis* were reported shortly after the introduction of this drug [37,18]. INH is the most prescribed drug for active infection and prophylaxis of TB [38]. INH is highly active against growing tubercle bacilli but not resting bacilli, with MIC in the range of 0.02 to 0.2μg mL^{-1}. It has a simple structure containing a pyridine ring and a hydrazide group, and both moieties are essential for its high activity against *M. tuberculosis*. A major target for INH has been shown to be the product of the *inhA* structural gene, which is located downstream of an ORF coding for a β-ketoacyl reductase (MabA) in the *inhA* operon [39]. The product of the *inhA* gene was shown to be an NADH-dependent enoyl-ACP (acyl carrier protein) reductase en-

zyme, which exhibits specificity for long chain (C_{18}>C_{16}) enoyl thioester substrates [40], which is consistent with its suggested involvement in mycolic acid biosynthesis. Consistent with InhA as the primary target of INH mode of action, inactivation of *M. smegmatis inhA*-encoded enoyl reductase and INH treatment resulted in similar mycolic acid biosynthesis inhibition, and morphological changes to the mycobacterial cell wall leading to cell lysis [41]. Consistent with these results, mutations in the *inhA* structural gene were identified in INH-resistant clinical isolates of *M. tuberculosis*. Recombinant InhA proteins with defined single aminoacids substitutions (I16T, I21V, I47T, I95P, and S94A – a spontaneous laboratory mutant that was later identified in clinical isolates) were expressed and purified to homogeneity, and showed by fluorescence spectroscopy to have higher dissociation constants for NADH than wild-type (WT) InhA, whereas there were only modest differences in the steady-state parameters [42]. Moreover, INH and ethionamide(ETH) resistance can be mediated by overexpression of *inhA* [43], and more recently, it was shown by specialized linkage transduction that the introduction of *inhA* (S94A) point mutation in *M. tuberculosis* confers clinically relevant levels of resistance to INH killing and inhibition of mycolic acid biosynthesis [44]. Biochemical and genetic evidence has been given likewise showing that InhA is the primary target of INH [45].

INH is a pro-drug that is activated by the mycobacterial *katG*-encoded catalase-peroxidase enzyme in the presence of manganese ions, NAD(H) and oxygen [42]. The KatG-produced acylpiridine fragment of INH is covalently attached to the C4 position of NADH (Fig. **3**) and forms a binary complex with the WT enoyl reductase of *M. tuberculosis* [46] with a dissociation constant value lower than 0.4 nM [47].

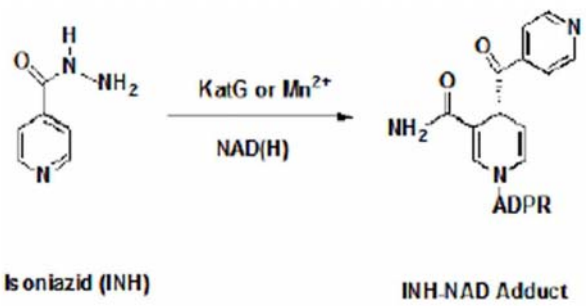

Fig. (3). Chemical structure of isoniazid and INH-NAD adduct that inhibits MtInhA activity.

The isonicotinyl-NAD^+ has been shown to be a slow, tight-binding competitive inhibitor of WT and INH-resistant InhA mutant enzymes [48]. The initial rapidly reversible weak binding (Ki = 16 nM) is followed by a slow isomerization process leading to a tighter enzyme-inhibitor complex with an overall dissociation constant (Ki^*) value of 0.75 nM. Approximately 50 % of INH-resistant clinical isolates of *M. tuberculosis* harbour deletions of, or missense mutations in, the *katG* gene that codes for a catalase-peroxidase enzyme [49, 50]. The S315T KatG mutant enzyme, which is one of the most commonly encountered substitutions in clinical INH-resistant strains, has been shown by isothermal titration calorimetry to have reduced affinity for INH as compared to WT KatG enzyme [51]. These authors have shown that although S315T KatG maintains reasonably good steady-state catalytic rates, poor binding of INH to the mutant enzyme would reduce INH activation and bring about drug resistance. The mechanism of action of INH is complex, as mutations in at least five different genes (*katG, inhA, ahpC, kasA, ndh*) have been found to correlate with INH resistance. It has recently been suggested that the acyclic 4*R* isomer of INH-NADP inhibits *M. tuberculosis* dihydrofolatre reductase, an enzyme essential for nucleic acid synthesis, prompting the authors to propose that this enzyme is also a target for isoniazid [52]. These findings could explain early reports describing the inhibition of nucleic acid by isoniazid in *M. tuberculosis* [53]. However, determination of a clinically relevant drug target requires the ability to transfer a single point mutation that causes drug resistance within a gene that putatively encodes a drug target and demonstrate that this transfer is sufficient, by itself, to confer drug resistance. To the best of our knowledge, it has been shown for InhA, thereby indicating that mycobacterial enoyl reductase is the target for INH mode of action [44].

More recently, we have shown by crystallographic studies that the INH-resistant mutant enzymes S94A, I47T and I21V structures in complex with NADH, solved to resolutions of 2.2 Å, 2.0 Å and 1.9 Å, respectively, have several structural modifications located in the active site, and which appear to indirectly affect, the dinucleotide binding loop structure. Moreover, pre-steady-state kinetics studies on binding of NADH were carried out, showing that the limiting rate constant values for NADH dissociation from the InhA-NADH binary complexes (k_{off}) were eleven, five and tenfold higher for, respectively, I21V, I47T and S94A INH-resistant mutants of InhA as compared to INH-sensitive WT InhA [54]. The correlation between NADH binding properties in solution, drug activation, crystallographic and kinetics studies provides a mechanism of resistance at molecular level for this clinically important drug.

4. AN INORGANIC COMPOUND AS ANTI-TB AGENT

Although the history of chemotherapeutic agent development demonstrates the remarkably successful tinkering of a few structural scaffolds by generations of medicinal chemists to meet the challenges of evolution of drug resistance, it also emphasizes the ongoing, cyclical need for innovation [55]. In view of the complicated mechanism of activation of INH, the increasing levels of clinically resistance to this drug, and the lack of introduction of new chemical entities to treat TB in the market for decades, new analogs of INH that overcome the mechanism of activation and are also active against drug-resistant strains of *M. tuberculosis* appear to be worthy of examination. Based on this challenge, a model system for *in vitro* activation of thioamide anti-TB drugs was proposed [56], in which a metal center containing a pentacyanoferrate(III/II) molecule attached to the ring of thioamide would promote an electron transfer (ET) reaction that mimics the *in vitro* activation of INH by KatG enzyme or Mn^{+2}. The rate constant, k_{et}=10 s^{-1}, was determined for this ET reaction. The rate of this reaction is strongly dependent on pH due to an acid-base equilibrium related to the deprotonation of the R-SH functional group of the imidothiol

form of thionicotinamide. Most of the INH resistance is associated with *KatG* structural gene alterations resulting in catalase-peroxidase mutant enzymes with impaired ability to form activated-INH intermediates. The oxidative activation of INH and ETH by cells of *M. tuberculosis* is mediated by the KatG and EthA enzymes, respectively, both via ET reaction that precedes inactivation of enzymes involved in mycolic acid biosynthesis [57]. One approach to overcome this mechanism is the use of low oxidation state metal complexes coordinated to the prodrugs. Accordingly, a new analog of INH that contains a pentacyanoferrate(III) moiety attached to the pyridine ring of INH (Fig. **4**), was shown to have inhibitory activity against INH-sensitive WT and INH-resistant I21V enoyl reductases of *M. tuberculosis* [58].

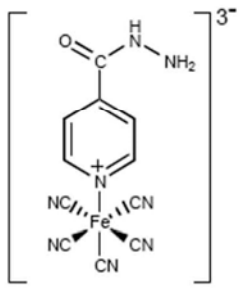

Fig. (4). Structural formula of pentacyano(isoniazid)ferrate(II) complex: $[Fe^{II}(CN)^5(INH)]^{3-}$.

Upon oxidation of $[Fe^{II}(CN)_5(INH)]^{3-}$ complex ($E_{1/2}$ = 549 mV *vs*. NHE) by oxygen and/or cellular oxidants, it is postulated that the thermodynamically unstable iron(III) complex would undergo a rapid intramolecular electron transfer reaction forming the $[Fe^{II}(CN)_5(isonicotinyl)]^{3-}$ intermediate species which could decay to the $[Fe^{II}(CN)_5(L)]^{3-}$ complex (L= isonicotinic acid, isonicotinamide, or isonicotinaldehyde) and bind to enoyl reductase resulting in inhibition of mycolic acid synthesis without the interference of KatG enzyme. Inactivation experiments demonstrate that the inhibition is time-dependent. Incubation of WT InhA with $Na_3[Fe^{II}(CN)_5(INH)]\cdot 4H_2O$ in the absence of NADH resulted in the time-dependent inactivation of the enzyme with an apparent first-order rate constant value of 327 (±34) x 10^{-3} min^{-1}, showing that the inorganic complex requires no activation by mycobacterial KatG, overcoming a major mechanism of resistance to INH. Moreover, the minimum inhibitory concentration (MIC) of $[Fe^{II}(CN)_5(INH)]^{3-}$ was determined radiometrically for *M. tuberculosis* $H_{37}Rv$ strain, displaying a value of 0.2 μg mL^{-1}, comparable to the MIC value for INH (0.02-0.2 μg mL^{-1}), and toxicity assays in HL60 leukemia and MCS-7 breast cancer cells yielded an IC_{50} value > 25mg mL^{-1}, thereby indicating a good selectivity index (SI = IC_{50}/MIC > 125). To a compound move forward through screening programs SI should be large than 10. These studies indicate that the mode of action of $[Fe^{II}(CN)_5(INH)]^{3-}$ compound requires no activation by KatG, no need for the presence of NADH, and is also effective against INH-resistant mutant InhA. More recently, we have shown that this inorganic complex is a slow-onset inhibitor of InhA, with an overall true inhibition constant value of 75 nM[59]. In addition, a half-time value of 630 min (10.5 h) for the limiting step for inhibitor dissociation from the binary complex was determined. Here we describe the slow-onset mechanism of binding of $[Fe^{II}(CN)_5(INH)]^{3-}$ to WT and INH-resistant I21V, S94A, and I47T mutant enoyl reductases, the dissociative half-life of the inorganic complex from the binary complex, and the overall inhibition constant for the mutant enzymes, showing that $[Fe^{II}(CN)_5(INH)]^{3-}$ is also a slow-onset inhibitor of the INH-resistant mutant enzymes. This inorganic complex represents a new class of leading compounds to the development of anti-tubercular agents aiming at inhibition of a validated molecular target.

4.1. Characterization of $[Fe^{II}(CN)_5(INH)]^{3-}$

The $Na_3[Fe^{II}(CN)_5(INH)].3H_2O$ complex was prepared by the direct reaction of $Na_3[Fe(CN_5)(NH_3)].3H_2O$ with isoniazid, in aqueous solution at room temperature, following a procedure reported for similar pentacyanoferrate(II) complexes with minor modifications [60]. Results of microanalysis of $Na_3[Fe^{II}(CN)_5(INH)].3H_2O$ compound yielded the following results: %C(exp)=28.2 (theor=28.4), %H (exp)=3.3 (theor=3.2), %N(exp)=23.8 (theor=24.0).

The ^1H NMR spectrum for the isoniazid free ligand presents two doublets. A downfield chemical shift of the doublet at δ 8.66 ppm with coupling constants (J) values of 1.65 Hz and 4.58 Hz, was assigned to the deshielded *ortho* hydrogen atoms of the pyridine ring. The upfield chemical shift of the doublet at δ 7.67 ppm with J values of 1.67 Hz and 4.58 Hz was attributed to the shielded *meta* hydrogen atoms of isoniazid. No signal was observed for the hydrogen atoms of the hydrazine substituent of the INH pyridine ring due to a rapid exchange with solvent.

The ^1H NMR spectrum of $Na_3[Fe^{II}(CN)_5(INH)].3H_2O$ complex presented the signals characteristic of the hydrogen atoms of the pyridine ring (δ 9.11 ppm for the *ortho* and δ 7.41 ppm for the *meta* hydrogen atoms). The features of the spectrum are consistent with the coordination of INH to the $[Fe^{II}(CN)_5]^{3-}$ metal center in the ratio 1: 1 via the nitrogen atom of the INH pyridine ring resulting in a deshielding of the *ortho* hydrogen atoms and shielding of *meta* hydrogen atoms due to the cyanide anisotropy and the (INH)$p\pi^* \leftarrow d\pi(Fe^{II})$ back-bonding. The anisotropy of the cyanides due to the perpendicular induced field at the C=N bonds inducts deshieldind of the *ortho* hydrogen atoms from the INH coordinated pyridine ring. This effect is more effective for the ortho-hydrogens due to the unfavorable distance between the cyanide ligands and the meta-hydrogens of the coordinated pyridine ring.

The Mössbauer spectrum of $Na_3[Fe^{II}(CN)_5(INH)]\cdot 3H_2O$ complex are doublets due to the presence of an electronic field gradient with non-cubic symmetry in the 57Fe nucleus [61]. The non-cubic electronic configuration of the central ion comes from the asymmetric σ and π bonding involving only the axial ligand L, reflecting on the isomer shift (d) Mössbauer parameter. The ligand σ donation mechanism increases the s electron population causing an increase of the electronic density on the metal [62]. The same effect is caused by the $p\pi^*$(INH) ← dπ (Fe) back-bonding that decreases the shielding effects. The σ and π bonding involving the metal and INH axial ligand are responsible for the appearance of the electric field gradient (EFG) at the ^{57}Fe nucleus. The quadrupole splitting is caused by the interaction

of the nuclear quadrupole moment of the iron atom with the Z component of the EFG. The Mössbauer parameters values ($\delta = 0.219 \pm 0.001$ mms^{-1}, $\Delta = 0.219 \pm 0.002$ mms^{-1}, referred to SNP) acquired for the $Na_3[Fe^{II}(CN)_5(INH)]\bullet 3H_2O$ complex strongly suggest the presence of an unique $^{57}Fe(II)$ Mössbauer nucleus, consistent with the proposed chemical compositions [63].

The most prominent feature of the electronic spectrum of the $[Fe^{II}(CN)_5(INH)]^{3-}$ complex is the band at 436nm ($\varepsilon = 4.0 \times 10^3$ M^{-1}cm^{-1}) assigned to the $[(INH)p\pi^* \leftarrow d\pi(Fe^{II})]$ metal-to-ligand charge transfer (MLCT) transition, suggesting a strong interaction between the metal ion and the nitrogen atom of the (INH) pyridine ring. The infrared (IR) vibrational spectrum of this inorganic complex displays bands at wavenumbers (cm^{-1}) associated with stretching frequencies of $\nu C{\equiv}N$ groups (2044 cm^{-1}), $\nu Fe^{II}{-}C$ (563 cm^{-1}), C–H bonds involving sp^2-hybridized carbons of the pyridine ring (3300 cm^{-1}), and C=O stretching (1668 cm^{-1}).

The cyclic voltamogram performed for the $Na_3[Fe^{II}(CN)_5INH].3H_2O$ complex in a 0.10 M CF_3CO_2Na aqueous solution, pH 3.5, shows waves ($E_{1/2} = 549$ mV versus NHE, at 50 mV s^{-1}) characteristic of a reversible one-electron process. The E_p values showed no dependence on the scan rate and the plot of i_p versus v1/2 was linear over the experimental range between 10 and 150 mV s^{-1}. Above the 549 mV potential, the unstable iron (III) precursor complex, formed by the action of oxygen and/or other cellular oxidants, is thermodynamically allowed to experiment a intramolecular electron transfer reaction originating the $[Fe^{II}(CN)_5(isonicotinyl)]$ intermediate species.

The $Na_3[Fe^{II}(CN)_5INH]\bullet 3H_2O$ complex showed to be stable at high acidic medium (pH $\leq$ 2.0) experimenting a reversible acid-base equilibrium of CN groups with a pKa = 2.3. The stability of the inorganic complex at acidic pH indicates that it has favourable characteristics to be administered orally, since it would not be degraded by the acidic pH of human digestive system.

4.2. Kinetics of $[Fe^{II}(CN)_5(INH)]^{3-}$ Binding to WT and INH-Resistant InhA Enzymes

To elucidate the mode of inhibition of the INH-sensitive WT and INH-resistant enoyl reductases by the inorganic complex, we performed binding experiments utilizing spectrofluorimetric techniques, through the observation of intrinsic protein fluorescence to measure enzyme-inhibitor complex(es) formation. As pointed out above, $[Fe^{II}(CN)_5(INH)]^{3-}$ acts as a slow-type binding inhibitor, based on classical slow-binding inhibition experiments [57] with an initial rapid formation of a binary complex between the enzyme and the inorganic compound (EI), which then undergoes a slow isomerization reaction to form EI*, in which the inhibitor is more tightly bound to the enzyme (Fig. **5**) as described for mechanism B by Morrison and Walsh [64]. To both distinguish between the three basic mechanisms of slow-binding inhibition and to obtain a reliable estimate of the rate and equilibrium dissociation constants for the enzyme-inhibitor complex formation, a simple and direct method in solution was developed, which only requires the enzyme and the inorganic complex. All the fluorescence experiments were carried out on a Shimadzu spectrofluorimeter, model RF-5301, connected to a thermostated bath, at 25°C. The fluorescence emission spectra of the proteins in the presence and in the absence of the inhibitor were performed in 100mM NaH_2PO_4 pH 7.5, in quartz cuvettes containing 2 μM of either WT, I21V, I47T or S94A InhA. The excitation wavelengths were 297, 298, and 299nm for WT, S94A, and I21V and I47T, respectively, and the fluorescence emission spectra were recorded at wavelengths ranging from 300 to 450nm. After recording the emission spectra of the proteins (intrinsic protein fluorescence spectrum in the absence of ligand), data were collected immediately following the addition of 100μM of $[Fe^{II}(CN)_5(INH)]^{3-}$ and 30 minutes after addition of inhibitor.

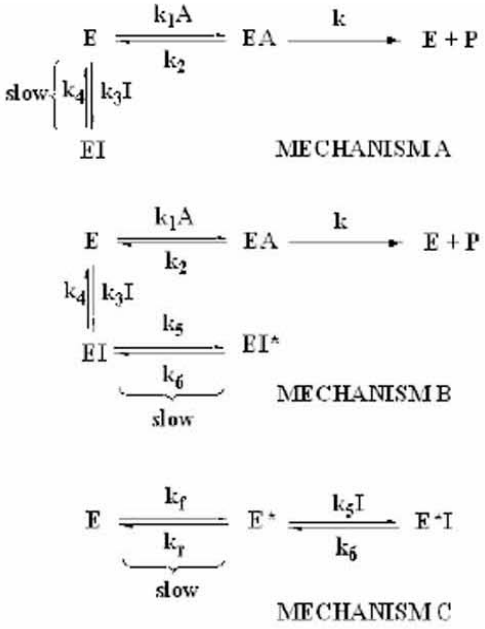

Fig. (5). Three basic mechanisms which account for reversible slow-binding inhibition of enzyme-catalyzed reactions.

As can be observed in the emission protein fluorescence spectrum for WT InhA (Fig. **6**), there is an initial rapid quench in protein fluorescence upon the addition of inhibitor, followed by a slow quench in protein fluorescence in the order of minutes, likely due to the slow formation of EI* complex(es), with the maximum wavelength of emission remaining unchanged at 335nm. This emission wavelength was chosen for the experiments of time-dependent quenching in protein fluorescence upon binding of $[Fe^{II}(CN)_5(INH)]^{3-}$ that provides a good estimate of the equilibrium dissociation constant (Ki) for the establishment of EI, and the rate constants k_5 and k_6, which represent the observed microscopic rate constants of direct and reverse isomerization of EI*. Time course assays were determined by continuously monitoring protein fluorescence quench for 15 minutes upon addition of varied inhibitor concentrations to protein solutions. We have observed that this time range is sufficient to allow the system reach equilibrium. Controls were carried out by following the same procedure in the absence of inhibitor. The slow step of quench in protein fluorescence, which is reported by an enzyme amino acid side chain (tryptophan), is likely due to previously suggested conformational changes in the active site of the enzyme upon formation of the binary complex [59].

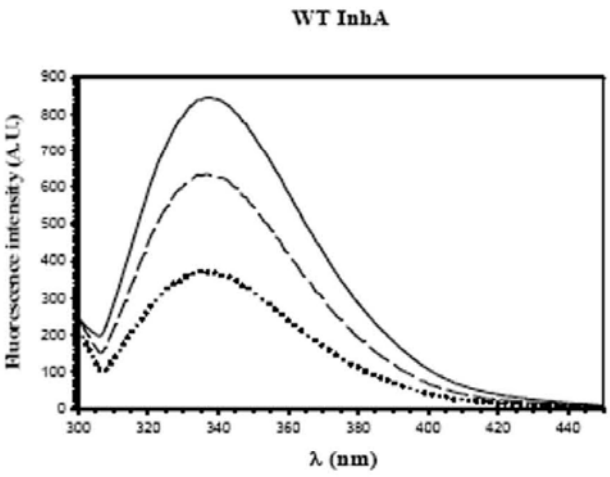

Fig. (6). Emission spectra of WT InhA. Solid line: sum of the fluorescence spectra of 2 μM WT InhA and 100 μM $[Fe^{II}(CN)^5(INH)]^{3-}$. Dashed line: fluorescence spectrum obtained immediately after mixing WT InhA and $[Fe^{II}(CN)^5(INH)]^{3-}$ at the final concentrations of 2 μM and 100 μM, respectively. Dotted line: Fluorescence spectrum obtained thirty minutes after mixing WT InhA and $[Fe^{II}(CN)^5(INH)]^{3-}$ the final concentrations of 2 μM and 100 μM, respectively.

A mechanism can be envisage in which inhibitor binding to the enzyme active site induces a conformational change that results in formation of a more stable enzyme-inhibitor complex from which the inhibitor is released at relatively slow rate [64]. In this context, the isomerization of the complex is directly related to the time-dependent quenching in protein fluorescence upon $[Fe^{II}(CN)_5(INH)]^{3-}$ binding to INH-sensitive WT and INH-resistant InhAs. Accordingly, the single exponential quench in protein fluorescence for each inhibitor concentration was fitted by non-linear regression to the following integrated equation [65]:

$$F = F_0 + a \exp(-k_{obs} t) \qquad [1]$$

where F and F_0 are, respectively, the protein fluorescence at time t and t_0, and a is the amplitude of the signal, and k_{obs} represents the apparent first-order rate constant for the establishment of the equilibrium between EI and EI^* complexes or the apparent isomerization rate constant for the formation of EI^*. A typical experimental trace obtained from the progress curves is shown in (Fig. **6**).

In an inhibition that conforms to mechanism A, it is assumed that the initial bimolecular interaction between enzyme and inhibitor is slow, and limited by the low value of the k_3 rate constant., which may be due to barriers that the inhibitor encounters in its binding to the enzyme active site. In mechanism B, the slow inhibition occurs after an initial interaction between enzyme and inhibitor to form a bimolecular complex EI, which then undergoes a slow isomerization reaction to form EI^* [64]. In mechanism C, a slow initial isomerization of two forms of free enzyme in solution (E and EI^*) is followed by a rapid binding of inhibitor to form E^*I complex. One of the graphical methods that allows to distinguish between the three slow-binding inhibition mechanisms (Fig. **5**) is a plot of the k_{obs} values versus inhibitor concentration [64]. A linear dependence in the plot of k_{obs} versus [I] is expected for mechanism A, for mechanism B this plot would

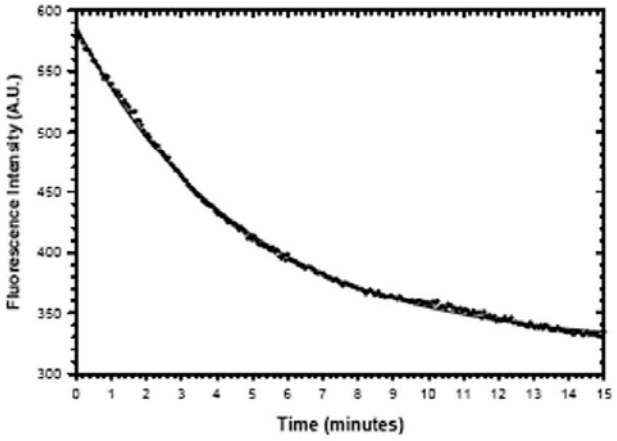

Fig. (7). Time-dependent binding 100μM $[Fe^{II}(CN)^5(INH)]^{3-}$ to 2μM S94A InhA. The solid curve represents the best fit of the data to equation [1]. Control experiments contained no inhibitor.

display a hyperbolic increase, and for mechanism C it would be described by a hyperbolic decrease with increasing inhibitor concentration. The plots for the WT and I21V, I47T and S94A InhA showed a hyperbolically increase pattern, which is consistent with mechanism B and allow us to confirm the previously determined mechanism of inhibition of WT InhA by the inorganic complex [59] and to extend this observation for the INH-resistant enzymes. If we assume that for mechanism B the bimolecular association process is faster than the unimolecular isomerization process (i.e. $k_3I+k_4 >> k_5+k6$), the concentration dependence of the apparent rate constants (k_{obs}) can be fitted to the following equation [66]:

$$k_{obs} = k_6 + k_5 [I]/Ki+[I] \qquad [2]$$

where Ki is the equilibrium dissociation constant for the formation of EI, k_5 and k_6 are the forward and reverse rate constants for the conversion of EI to EI^*, respectively. Data for WT, I21V, I47T and S94A InhAs fitted very well to equation **[2]** (Fig. **8**). Unfortunately, reliable estimates for the reverse isomerization rate constant could not be obtained probably because the low k_6 values that cannot be determined from the binding results and thus a direct method was employed as described in the next section. On the other hand, reliable values could be obtained for the dissociation constant and forward rate constant, which are shown in (Table **1**). One can observe that the Ki and k_5 values for WT InhA (86 ± 15 μM and 0.42 ± 0.02 min^{-1}, respectively) are in good agreement (within the standard error) with the values obtained from experiments of time-dependent inactivation of WT InhA by varied concentrations of $[Fe^{II}(CN)_5(INH)]^{3-}$ (73 ± 14 μM and 0.51 ± 0.03 min^{-1}) [59], thereby supporting the robustness of the data and the validity of the method used for analysis. The values of the forward rate constants for the EI^* formation of by the inorganic complex with WT, I47T, and I21V are 3.2, 4.4 and 2.7 fold higher than the value determined for activated INH [48]. Moreover, the results presented here show that the inorganic compound binds to InhA enzymes with no need for activation, in contrast to INH that requires activation by KatG to form the INH-NAD adduct in agreement with unsuccessful attempts to show INH binding to either InhA or InhA-NADH complex by titration microcalorimetry [67]. Since mutations in the *katG* gene have been

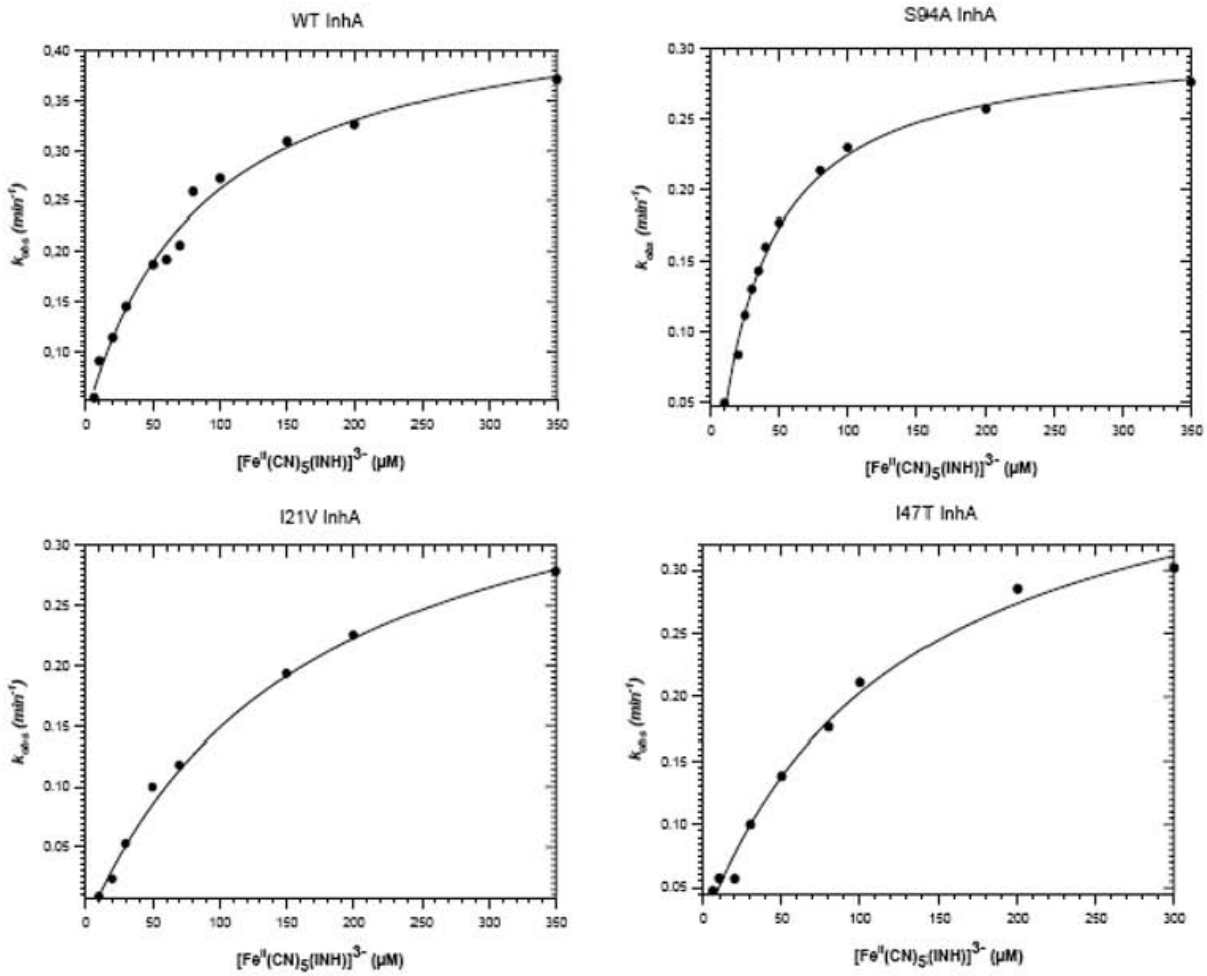

Fig. (8). Determination of dissociation constant (Ki) for the rapidly reversible EI complex and forward rate constant (k5) for WT and INH-resistant InhA enzymes. The values of Ki and k5 were obtained from plotting apparent pseudo-first order rate constant (kobs) as a function of $[Fe^{II}(CN)^5(INH)]^{3-}$ and fitting the data to equation [2].

Table 1. Kinetic Constants for the Binding of Wt and Mutant InhA by $[Fe^{II}(CN)_5(INH)]^{3-}$

Enzyme	WT InhA	S94A InhA	I21V InhA	I47T InhA
Ki (μM)	86 ± 15	44 ± 9	75 ± 21	104 ± 24
k_5 (min^{-1})	0.42 ± 0.02	0.31 ± 0.01	0.36 ± 0.01	0.41 ± 0.03

associated with decreased susceptibility to INH in approximately 50% of clinical isolates of *M. tuberculosis* [49], the inorganic compound described here could overcome this mechanism of INH resistance.

4.3. Dissociation of $[Fe^{II}(CN)_5(INH)]^{3-}$ from I21V, S94A and I47T InhA and Overall Inhibition Constant (Ki^*)

In the field of drug discovery, especially in the search for enzyme inhibitors, the focus is usually on the binding event because enzymes are catalysts. They make and break specific covalent chemical bonds, in contrast with other drug targets, such as cell surface receptors, ion channels, transporters, nuclear hormone receptor, and DNA, that do not. Enzyme catalysis progress through binding events, conformational changes, one or more transition states, or reaction intermediates, and product release, and all of these steps occur with defined rate constants [68]. Accordingly, a chemical compound that disturb this system or mimic one or more of the catalytic steps, leading to the formation of a dead-end complex with the enzyme, should be considered as a new candidate for drug development. However, there are several pharmacologycal factors that influence the *in vivo* efficacy of an enzyme inhibitor, especially those that precede the binding of the compound to its molecular target, such as absorption, systemic distribution, and clearance. These factors af-

fect directly the local concentration of ligand that arrives at the receptor-harbouring tissue and therefore the rate of encounter between a dosed ligand and a tissue-associated receptor [69].

Although the rate of enzyme-inhibitor complex formation can have an important impact on the pharmacology of a drug, it is also influenced by the above mentioned constraints. In contrast, after the establishment of the equilibria involving the EI complex, these pharmacological factors cannot have any influence on the complex dissociation rate, which is also independent of the local concentration of ligand. The InhA-$[Fe^{II}(CN)_5(INH)]^{3-}$ complex(es) formation involves a conformational change to a form in which the inhibitor is more tightly bound, probably due to a protein conformational change. The reverse isomerization rate constant (k_6) , which limits the inhibitor dissociation, is entirely dependent on specific interaction (such as changes in protein conformation, nonpolar forces, hydrogen bonds, van der Waals interactions and so on) between the ligand and its target binding pocket. Copeland and coworkers thus proposed that *in vitro* measurement of the dissociative half-life is a crucial metric of compound optimization, and could be a key indicator of *in vivo* duration of efficacy [69]. The dissociative half-life can be directly estimated if the value of k_6 is known, using the simple relationship half-life=0.693/k_6 [70].

Accordingly, to both demonstrate reversible binding and to obtain reliable estimates for k_6 values for S94A, I21V and I47T InhAs and $[Fe^{II}(CN)_5(INH)]^{3-}$ binary complexes, experiments of recovery of biological activity were carried out on these inhibitory complexes [71]. These experiments consist of combining the free enzyme and inhibitor at high concentrations and let the system reach equilibrium, followed by rapid dilution into a solution containing both substrates at near-saturating concentrations to perturb the equilibrium between enzyme and inhibitor. As the inhibitor dissociates from the enzyme it becomes available to react with substrates and to contribute to the assay signal. Since previous studies showed that $[Fe^{II}(CN)_5(INH)]^{3-}$ act as a competitive inhibitor of WT InhA with respect to NADH and DD-CoA [59], it was anticipated that the same behavior would be followed by the mutant enzymes, and thus the conditions of the experiments were as previously described, with some minor modifications. Briefly, the S94A*, I21V*, I47T*-$[Fe^{II}(CN)_5(INH)]^{3-}$ binary complexes were formed by incubation of 25 μM mutant enzymes with 125 μM of $[Fe^{II}(CN)_5(INH)]^{3-}$, in 100 mM NaH_2PO_4 pH 7.5, in a final volume of 200 μL, and incubated at 25°C for 5 hours. After preincubation, all the samples were diluted into assay mixtures containing the following components: 85 μM DD-CoA, 250μM NADH, 8% (vol/vol) glycerol, 0.1 mg mL^{-1} BSA, in 100 mM NaH_2PO_4 pH 7.5. The regain of enzymatic activity was followed by monitoring for 6 hours the absorbance decrease at 340 nm due to NADH oxidation. The final concentrations of enzymes were in the range of 0.75 - 1.5 nM. Glycerol and BSA were added to the assay mixture to confer enzyme stability, since the WT and mutants of InhA showed no activity at concentrations below 3 nM without the addition of these components. Measurements of absorbance at 340 nm in control experiments containing no inhibitor and NADH degradation due to long light exposure were subtracted from the final progress curves. The time courses of activity regain for S94A, I21V and I47T enzymes were fitted to the following equation [64]:

$$A_t = A_0 - v_s t - (v_i - v_s)(1 - \exp(-k_6 t)/ k_6 \quad [3]$$

where A_t and A_0 are, respectively, the absorbance at time t and 0, v_i and v_s represent the initial velocity and the final steady-state velocity, respectively, and k_6 is the reverse isomerization rate constant for conversion of EI^* to EI. The enzyme activity regain experiment was carried out at a single $[Fe^{II}(CN)_5(INH)]^{3-}$ concentration because it was previously demonstrated that different concentrations of the inhibitor in the preincubation mixture yielded similar values for k_6 [59], and dilution into a relatively large volume of assay containing near-saturating concentrations of both substrates gives rise to a condition where the final inhibitor concentration in the assay mixtures and/or its effects are negligible. Values of 1.2 (± 0.1) x 10^{-3} min^{-1}, 1.27 (± 0.2) x 10^{-3} min^{-1} and 1.45 (± 0.2) x 10^{-3} min^{-1}, for, respectively, I47T, I21V and S94A were determined for k_6 (Fig. **9**).

The half-life ($t_{½}$) for the inhibitor dissociation from E^*-$[Fe^{II}(CN)_5(INH)]^{3-}$ binary complexes were estimated to be 578 min, 546 min and 478 min for I47T, I21V and S94A, respectively, which are in good agreement with the value determined for WT InhA (630 min) [59]. The overall dissociation constant (Ki^*) is a function of the relative magnitudes of forward (k_5) and reverse (k_6) rate constants for the isomerization process of $InhA^*$- $[Fe^{II}(CN)_5(INH)]^{3-}$ binary complex and the equilibrium dissociation constant (Ki). The overall dissociation constant can be calculated by using the relationship $K_i^* = K_i k_6/(k_5+k_6)$. To calculate Ki^* for WT and mutant InhAs, the Ki and k_5 values from the binding experiments, k_6 values from activity regain of mutant enzymes described here, and the value of 1.1 x 10^{-3} min^{-1} previously for WT InhA [59] were substituted into the $K_i^* = K_i k_6/(k_5+k_6)$ relationship. Ki^* values of 225, 205, 263 and 303 nM were estimated for, respectively, WT, S94A, I21V and I47T InhA enzymes, showing that the residues substitutions in the mutant enzymes result in insignificant effects on the inorganic complex affinity. Moreover, in a slow inhibition that conforms to mechanism B, Ki^* must be much less than Ki, and also the reverse isomerization rate constant (k_6) must be less than the forward isomerization rate constant (k_5) [72], conditions that are satisfied by the $[Fe^{II}(CN)_5(INH)]^{3-}$ inhibition.

Slow rates of dissociation are expected to enhance inhibitor effectiveness, since the intervals between the doses can be longer. A comparison between $t_{½}$ values for $[Fe^{II}(CN)_5(INH)]^{3-}$ and for the INH-NAD adduct [48] shows that the former dissociates from INH-sensitive WT and INH-resistant I47T, I21V and SI4A mutants more slowly than the latter. This observation combined with the fact that the compound also forms the EI^* complex more rapidly, as shown in the previous section, suggest that $[Fe^{II}(CN)_5(INH)]^{3-}$ is a promising anti-TB agent.

5. CONCLUDING REMARKS

In the field of TB drug discovery and development, the search for analogs of INH appears worthy of examination as antitubercular agents, given the chemical simplicity of this molecule, its favourable bioavailability and toxicity profiles. However, the need for activation and the growing levels of

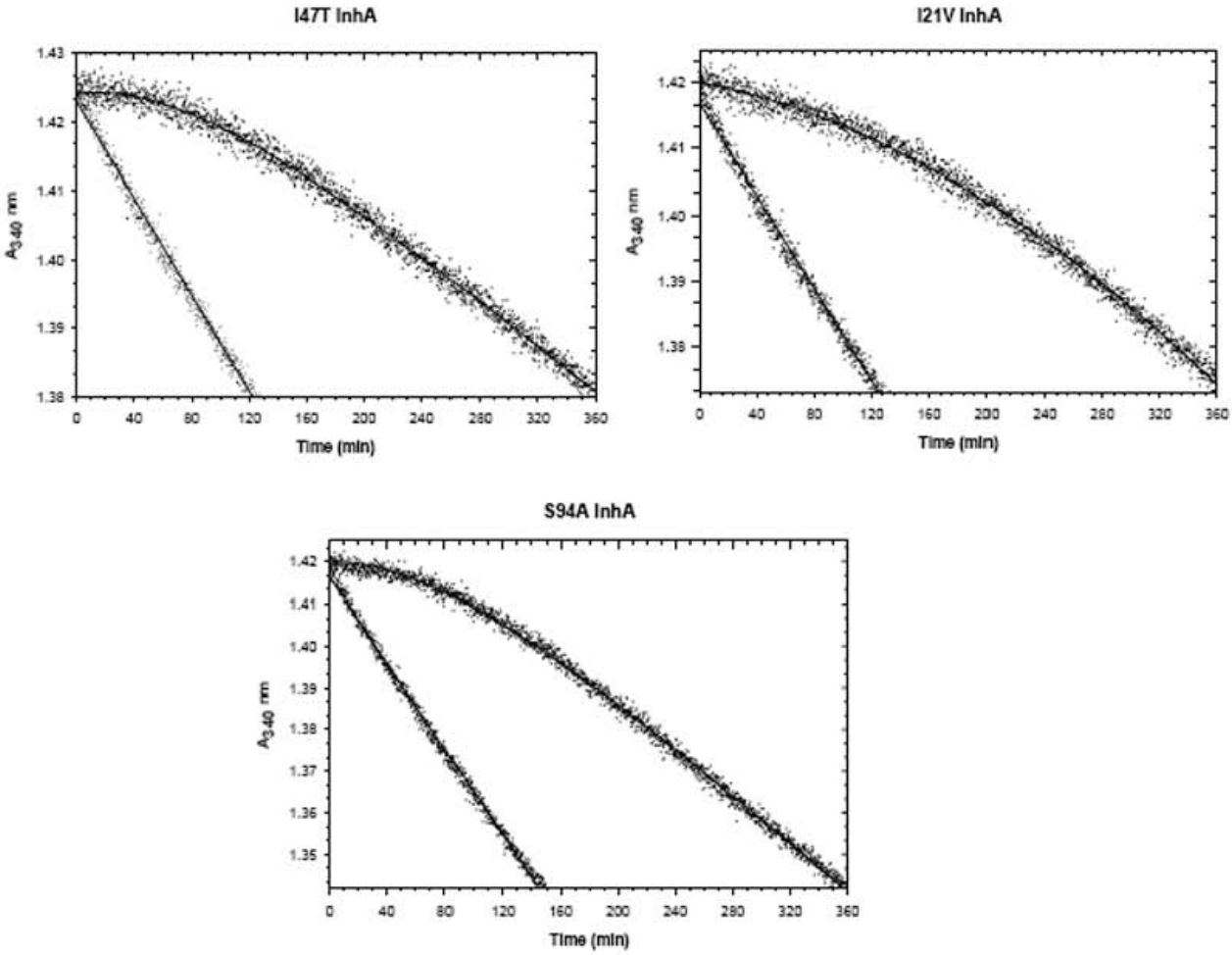

Fig. (9). Dissociation of [FeII(CN)5(INH)]3- from INH-resistant enoyl reductases I47T I21Vand S94A. Enzyme (25μM) was incubated with 125μM of $[Fe^{II}(CN)^{5}(INH)]^{3-}$ for 5h at 25°C. Samples were diluted into assay mixtures containing near-saturating concentrations of both substrates, and the activity regain monitored at 340nm for 6h.

resistance present new challenges that need to be overcome by new compounds derived from INH basic structure. The inorganic complex described in this work is a promising candidate for further drug development, since it needs no activation by KatG or other enzyme and no need for the formation of any kind of adduct with the cofactor NAD(H) to bind to its molecular target, the *M. tuberculosis* InhA. Moreover, the compound is also active and binds in a similar fashion to INH-resistant clinical isolates harboring inhA-structural gene mutations, showing similar dissociation and rate constants for the establishment of the EI complex compared to the WT enzyme. And even more important, after the formation of the final EI^{*} complex, its display a long residence time in the active site of the enzymes, which is a desirable feature for a drug to have a useful *in vivo* efficacy. The drug design strategy presented here, which consists of the coordination of the ligand to a metal center, is of special interest because, as pointed out by Gerard Jaouen, the bioinorganic chemistry discipline "needs to prove it can create something useful for society" [73]. The recent development of a series of compounds consisting of ciprofloxacin and enoxacin coordinated to Cu(II)and Co(II) were shown to active against several pathogens (*S. aureus*, *E. faecalis*, *B. subtilis*) with MIC values similar, or in some cases lower than, the corresponding free ligands [74]. Metal conjugation with copper and iron to N^{1}-benzylidene-pyridine carboxamidrazones, a new class of chemotherapeutic agents, results in 32-64 fold enhancement in antitubercular activity against drug-susceptible *M. tuberculosis* $H_{37}Rv$, and two of this compounds (MC_1 and MC_9) have MICs in the of 2 to 4 μM, which are comparable to those for INH [75]. Based on the ability to cause enhancement in the antimalarial activity of chloroquine by incorporation of a ferrocenyl moiety on the side chain, a series of ferrocenyl diamino alcohols and diamines were synthesized and showed to be active against *M. tuberculosis*, and the replacement of the ferrocenyl group with the phenyl group results in complete loss of the anti-TB activity, which confirms the importance of the introduction of the ferrocene in the diamine structure [76]. We hope that the data and approach described here will bear fruit and allow the development of new antitubercular agents to treat drug-sensitive and –resistant strains of *M. tuberculosis*.

ACKNOWLEDGMENTS

Financial support for this work was provided by Millenium Initiative Program MCT-CNP, Ministry of Health-Department of Science and Technology (DECIT)-UNESCO

(Brazil) to D.S.S. and L.A.B. and L.A.B. also acknowledge grants awarded by CNPq, FINEP, and PRONEX/ FAPERGS/CNPq. D.S.S. (CNPq, 304051/1975-06) and L.A.B. (CNPq, 520182/99-5) are researchers awardees from the National Research Council of Brazil. Financial support was also provided by Laboratório Americano de Farmacoterapia S.A. (FARMASA). Authors inform that there is a patent pending.

ABBREVIATIONS

ACP	=	Acyl carrier protein
CoA	=	Coenzyme A
DD-CoA	=	2-*Trans*-dodecenoyl coenzyme A
DOTS	=	Directly observed treatment short course
ET	=	Electron transfer
ETH	=	Ethionamide
FAS	=	Fatty acid biosynthesis system
HIV	=	Human immunodeficienty virus
INH	=	Isoniazid
InhA	=	2-*trans*-enoyl-ACP (CoA) reductase
KatG	=	Catalase-peroxidase
MabA	=	β-Ketoacyl reductase
MDR	=	Multi-drug resistant
MIC	=	Minimum inhibitory concentration
NADH	=	Nicotinamide adenine dinucleotide
TB	=	Tuberculosis
WHO	=	World health organization
XDR	=	Extensively-drug resistant

REFERENCES

[1] Bloom, B.R.; Myrray, C.J.L. *Science*, **1992**, *257*, 1055.
[2] Gutierrez, M.C.; Brisse, S.; Brosch, R.; Fabre, M.; Omaïs, B.; Marmiesse, M.; Supply, P.; Vincent, V. *PloS Pathog.*, **2005**, *1(e5)*, 55.
[3] Young, D.B.; Marshall, B.; Smet, K.D. The return of the resistant microbes, in: The Diagnostic Challeng, **1996**, E.P.Fischer and S.Klose, eds., Boehringer Mannheim Gmb, Mannheim.
[4] Raviglione, M.C. *Tuberculosis*, **2003**, *83*, 4.
[5] World Health Organization. Global Tuberculosis Control Report, **2006.**
[6] Dye, C.; Scheele, S.; Dolin, P.; Pathania, V.; Raviglione, M.C. *JAMA*, **1999**, *282*, 677.
[7] Reid, A.; Scano, F.; Getahun, H.; Willians, B.; Dye, C.; Nunn, P.; De Cock, K.M.; Hankins, C.; Miller, B.; Castro, K.G.; Raviglione, M.C. *Lancet Infect. Dis*, **2006**, *6*, 483.
[8] Corbett, E.L.; Watt, C.J.; Walker, N.; Maher, D.; Williams, B.G.; Raviglione, M.C.; Dye, C. *Arch.Intern.Med.*, **2003**, *163*, 1009.
[9] World Health Organization. Guidelines for the programmatic management of drug-resistant tuberculosis, **2006.**
[10] World Health Organization. XDR-TB – Extensive Drug Resistant TB. **2006.**
[11] Duncan, K. *Tuberculosis*, **2003**, *83*, 201.
[12] Grosset, J. *Clin. Chest Med.*, **1980**, *1*, 231241.
[13] Hiriyanna, K.T.; Ramakrishnan, T. *Arch. Microbiol.*, **1986**, *144*, 105.
[14] Russel, D.G. *Nat. Rev. Mol. Cell Biol.*, **2001**, *2*, 1.
[15] Hingley-Wilson, S.M.; Sambandamurthy, V.K.; Jacobs, W.R.Jr. *Nat. Immunol.*, **2003**, *4*, 949.
[16] Schatz, A.; Waksman, S.A. *Proc. Soc. Exp. Biol. Med.*, **1944**, *57*, 244.
[17] Kushner, S.; Dalalian, H.; Sanjurjo, J.L.; Bach, F.L.; Safir, S.R.; Smith, V.K.Jr.; Williams, J.H. *J. Am. Chem. Soc.*, **1952**, *74*, 3617.
[18] Middlebrook, G. *Am. Rev. Tuberc.*, **1952**, *65*, 765.
[19] Mitchison, D.A. *Tubercle*, **1985**, *66*, 219.
[20] World Health Organization. *WHO document WHO/CDS/TB/2001.285*, **2001**, Geneva.
[21] Pablos-Méndez, A.; Gowda, D.K.; Frieden, T.R. *Bull. World Health Organ.*, **2002**, *80*, 489.
[22] Takayama, K.; Wang, C.; Besra, G.S. *Clin. Microb. Rev.*, **2005**, *18(1)*, 81.
[23] Brennan, P.J. *Tuberulosis.*, **2003**, *83*, 91.
[24] Brennan, P.J.; Nikaido, H. *Annu. Rev. Biochem.*, **1995**, *64*, 29.
[25] Barry III, C.E.; Boshoff, H.I. *Drug.Disc. Today: Dis. Mech.*, **2006**, *3(2)*, 237.
[26] Schroeder, E.K.; de Souza, O.N.; Santos, D.S.; Basso, L.A. *Curr. Pharm. Biotechnol.*, **2002**, *3(3)*, 197.
[27] Basso, L.A.; Santos, D.S. *Med. Chem. Rev.*, **2005**, *2*, 393.
[28] Watanabe, M.; Aoyagi, Y.; Mitome, H.; Fujita, T.; Naoki, H.; Ridell, M.; Minnikin, D.E. *Microb.*, **2002**, *148*, 1881.
[29] Boissier, F.; Bardou, F.; Guillet, V.; Uttenweiler-Joseph, S.; Daffé, M.; Quémard, A.; Mourey, L. *J. Biol. Chem.*, **2006**, *281(7)*, 4434.
[30] Besra, G.S.; Kremer, L. In Tuberculosis and the Tubercle Bacillus; Cole, S.T.; Eisenach, K.D.; McMurray, D.N.; Jacobs, W.L.Jr., Eds.; ASM Press: Washington, **2005**, pp. 287-305.
[31] Cronan, J.E.; Rock, C.O. In Escherichia coli and Salmonella: Cellular and Molecular Biology; Neidhardt, F.C., Ed.; ASM Press: Washington, **1996**, pp. 612-636.
[32] Brindley, DN; Matsumura, S.; Block, K. *Nat.*, **1969**, *224*, 666.
[33] Bloch, K. *Methods Enzymol.*, **1975**, *35*, 84.
[34] Slayden, R.A.; Barry III, C.E. *Tuberculosis*, **2002**, *82*, 149.
[35] Veyron-Churlet, R.; Bigot, S.; Verdoux, O.G.S.; Malaga, W.; Daffé, M.; Zerbib, D. *J. Mol. Biol.*, **2005**, *353*, 847.
[36] Meyer, H.; Mally, J. *Mont. für Chem.*, **1912**, *33*, 393.
[37] Fox, H.H. *Chem. Eng. News*, **1951**, *29*, 3963.
[38] Basso, L.A.; Blanchard, J.S. *Adv. Exp. Med. Biol.*, **1998**, *456*, 115.
[39] Banerjee, A.; Dubnau, E.; Quémard, A.; Balasubamanian, V.; Um, K.S.; Wilson, T.; Collins, D.; de Lisle, G.; Jacobs, W.R.Jr. *Science*, **1994**, *263*, 227.
[40] Quémard, A.; Sacchettini, J.C.; Dessen, A.; Vilchéze, C.; Bittman, R.; Jacobs, W.R.Jr.; Blanchard, J.S. *Biochem.*, **1995**, *34*, 8235.
[41] Vilchéze, C.;Morbidoni, H.R.; Weisbrod, T.R.; Iwamoto, H.; Kuo, M.; Sacchettini, J.C.; Jacobs, W.R.Jr. *J. Bacteriol*, **2000**, *182*, 4059.
[42] Basso, L.A.; Zheng, R.; Musser, J.M.; Jacobs, W.R.Jr.; Blanchard, J.S. *J. Infect. Dis.*, **1998**, *178*, 769.
[43] Larsen, M.H.; Vilchéze, C.; Kremer, L.; Besra, G.S.; Parsons, L.; Salfinger, M.; Heifets, L.; Hazbon, M.H.; Alland, D.; Sacchettini, J.C.; Jacobs, W.R.Jr. *Mol. Microb.*, **2002**, *46*, 453.
[44] Vilchèze, C.; Wang, F.; Arai, M.; Hazbón, M.H.; Colangeli, R.; Kremer, L.; Weisbrod, T.R.; Alland, D.; Sacchettini, J.C.; Jacobs, W.R.Jr. *Nat. Med.*, **2006**, *12*, 1027.
[45] Kremer, L; Dover, L.G.; Morbidoni, H.R.; Vilchéze, C.; Maughan, W.N.; Baulard, A.; Tu, S.-C.; Honoré, N.; Deretic, V.; Sacchettini, J.C.; Locht, C.; Jacobs, W.R.Jr.; Besra, G.S. *J. Biol. Chem.*, **2003**, *278*, 20547.
[46] Rozwarski, D.A.; Grant, G.A.; Barton, D.H.R.; Jacobs, W.R.Jr.; Sacchettini, J.C. *Sci.*, **1998**, *279*, 98.
[47] Lei, B.; Wei, C.J.; Tu, S.C. *J. Biol.Chem.*, **2000**, *275*, 2520.
[48] Rawat, R.; Whitty, A.; Tonge, P.J. *Proc. Nac. Acad. Scienc. USA.*, **2003**, *100*, 13881.
[49] Ramaswamy, S.V.; Reich, R.; Dou, S.-J.; Jasperse, L.; Pan, X.; Wanger, A.; Quitugua, T.; Graviss, E.A. *Antimicrob. Agents Chemother.*, **2003**, *47*, 1241.
[50] Heym, B.; Alzari, P.M.; Honoré, N.; Cole, S.T. *Mol. Microbiol.*, **1995**, *15*, 235.
[51] Yu, S.; Girotto, S.; Lee, C.; Magliozzo, R.S. *J. Biol. Chem.*, **2003**, *278*, 14769.
[52] Argyrou, A.; Vetting, M.W.; Aladegbami, B.; Blanchard, J.S. *Nat. Struct. Mol Biol.*, **2006**, *13*, 408.
[53] Gangadharam, P.R.; Harold, F.M.; Schaefer,W.B. *Nat.*, **1963**, *198*, 712.
[54] Oliveira, J.S.; Pereira, J.H.; Canduri, F.; Rodrigues, N.C.; Souza, O.N.; Azevedo, W.F.Jr.; Basso, L.A.; Santos, D.S. *J. Mol. Biol.*, **2006**, *359*, 646.
[55] Walsh, C. *Nat. Rev. Microbiol.*, **2003**; *1*, 65.

[56] Souza, E.H.S.; Pontes, D.L.; Diógenes, I.C.N; Lopes, L.G.F.; Oliveira, J.S.; Basso, L.A.; Santos, D.S.; Moreira, I.S. *J. Inorg. Biochem.*, **2005**, *99*, 368.
[57] DeBarber, A.E.; Mdluli, K.; Bosman, L.G.; Bekker, L.G.; Barry III, C.E. *Proc. Natl. Acad. Sci. USA*, **2000**, *97*, 9677.
[58] Oliveira, J.S.; Sousa, E.H.S.; Basso, L.A.; Palaci, M.; Dietze, R.; Santos, D.S.; Moreira, I.S. *Chem. Comm.*, **2004**, *3*, 312.
[59] Oliveira, J.S.; Sousa, E.H.S.; Souza, O.N.; Moreira, I.S.; Santos, D.S.; Basso, L.A. *Curr. Pharm. Des.*, **2006**, *12*, 2409.
[60] Moreira, I.S.; Franco, D.W.; *Inorg. Chem.*, **1994**, *33*, 1607.
[61] Coelho, A.L.; Moreira, I.S.; Araújo, J.H.; Araújo, M.A.B. *J.Radioanal. Nucl. Chem.*, **1989**, *136*, 299.
[62] Dickson, D.P.E.; Berry, F.J. Mössbauer Spectroscopy, Cambridge University Press, London, **1986.**
[63] Moreira, I.S.; Lima, J.B.; Franco, D.W. *Coord. Chem. Rev.*, **2000**, *196*, 197.
[64] Morrison, J.F.; Walsh, C.T. *Adv. Enzymol.Relat.Areas Mol. Biol.*, **1988**, *61*, 201.
[65] Sculley, M.J.; Morrison, J.F.; Cleland, W.W. *Biochim. et Biophys. Ac.*, **1996**, *1298*, 78.
[66] Nakatani, H.; Hiromi, K. *J. Biochem.*, **1980**, *87*, 1805.
[67] Johnsson, K.; Schultz, P.G. *J. Am. Chem. Soc.*, **1994**, *116*, 7425.
[68] Robertson, J.G. *Biochem.*, **2005**, *44(15)*, 5561.
[69] Copeland, R.A.; Pompliano, D.L.; Meek, T.D. *Nat. Rev. Drug Discov.*, **2006**, *5*, 730.
[70] Copeland, R.A. Evaluation of Enzyme Inhibitors in Drug Discovery: a Guide for Medicinal Chemists and Pharmacologists, Wiley: New York, **2005.**
[71] Williams, J.W.; Morrison, J.F.; Duggleby, R.G. *Biochem.*, **1979**, *18*, 2567.
[72] Copeland, R.A. Enzymes – A Practical Introduction to Structure, Mechanism, and Data Analysis, Wiley: New York, **2000.**
[73] Dagani, R. The bio side of organometallics. *Chem.Eng.News*, **2002**; *80*, 23.
[74] Jiménez-Garrido, N.; Perelló, L.; Ortiz, R.; Alzuet, G.; González-Álvarez, M.; Cantón, E.; Liu-González, M.; García-Granda, S.; Pérez-Priede, M. *J. Inorg. Biochem.*, **2005**, *99*, 677.
[75] Sandbhor, U.; Padhye, S.; Billington, D.; Rathbone, D.; Franzblau, S.; Anson, C.E.; Powell, A.K. *J. Inorg. Biochem.*, **2002**, *90*, 127.
[76] Razafimahefa, D.; Ralambomanana, D.A.; Hammouche, L.; Pélinski, L.; Lauvagie, S.; Bebear, C.; Brocard, J.; Maugein, J. *Bioorg. Med. Chem. Lett.*, **2005**, *15*, 2301.

Received: November 20, 2006 **Revised: April 20, 2007** **Accepted: Apri 20, 2007**

3. Considerações Finais

A TB humana é a doença causada por um único agente infeccioso responsável pela maior taxa de mortalidade na atualidade. O microorganismo causador desta doença, *Mycobacterium tuberculosis*, que acompanha o ser humano há milênios e que possui um alto poder de adaptação às defesas do organismo hospedeiro, foi o responsável por milhares de mortes no passado quando não havia nenhum conhecimento sobre as causas da doença.

Este panorama começou a ser revertido no final do século XIX, quando Robert Koch identificou o seu agente causador. Nesta época, já existia o conhecimento de que a doença era transmissível. No entanto, apenas na metade do século XX é que surgiram os primeiros agentes para tratar a TB, como a INH e a pirazinamida. Com a introdução posterior de outras drogas, entre elas, rifampicina e etambutol, foi possível criar um esquema terapêutico eficaz para controlar e combater a doença.

Durante décadas, observou-se uma queda das taxas de novos casos e de mortalidade em países desenvolvidos e uma estabilização destes indicadores em países subdesenvolvidos. De fato, pensava-se que a TB poderia ser eliminada até o fim do século XX. No entanto, no final da década de 80 e início da década de 90, esse quadro começou a sofrer um revés no mundo todo, em especial em países desenvolvidos, principalmente, nos EUA, com o surgimento e a disseminação de cepas resistentes a múltiplas drogas (MDR-TB). Nesta época, começou a ser discutida e aplicada a prática da detenção involuntária, principalmente, na cidade de Nova York (EUA). Esta prática consistia na restrição do direito universal de ir e vir dos pacientes diagnosticados com MDR-TB, sendo os mesmos obrigados pelo Estado a permanecerem internados em instituições de saúde durante o período de tratamento, a fim de que não disseminassem pela sociedade estas cepas de TB

resistentes. O tratamento destes pacientes foi possível graças à existência das drogas de segunda linha, mais tóxicas e de maior custo que as de primeira linha.

Nesta época, mais precisamente em 1993, a TB foi declarada pela Organização Mundial da Saúde uma emergência à saúde global, sendo necessários esforços urgentes para o controle da doença, como o desenvolvimento de novos fármacos, otimização dos métodos de diagnóstico e determinação de suscetibilidade a drogas, políticas públicas de distribuição e de estoque adequado de medicamentos, além de um rigoroso controle e vigilância direta sobre a terapia aplicada aos pacientes. Alguns destes objetivos puderam ser alcançados, em parte, pela disseminação da aplicação do sistema DOTS de tratamento da TB.

No entanto, mais recentemente, a ocorrência de resistência às drogas em *M.tuberculosis* está se tornando uma grave ameaça ao controle da doença. De acordo com o relatório anual de controle global da TB de 2006, da OMS (1), durante o ano de 2004, aproximadamente 17% (460.000) de todos os novos casos mundiais eram MDR-TB. Mais preocupante é o surgimento do que tem sido denominado de TB extensivamente resistente às drogas (XDR-TB) (2,3), que preocupa epidemiologistas e profissionais da saúde com a possível ameaça do retorno do tratamento da TB à era pré-quimioterápicos quando ,aproximadamente, 50% dos pacientes faleciam.

A definição revisada de XDR-TB é a doença causada por bactéria que é resistente a pelo menos INH e rifampicina – resistência que define as cepas MDR-TB – com a adição de resistência a qualquer fluoroquinolona e ao menos a uma droga de segunda linha injetável (amicacina, capreomicina ou canamicina) (4). A ocorrência de resistência às fluoroquinolonas e às drogas injetáveis implica na perda das mais potentes e menos tóxicas opções de quimioterapia de segunda linha para o tratamento da TB. Infelizmente, um número significativo de cepas XDR-TB estão

indo além da definição de XDR-TB e são essencialmente incuráveis, sendo resistentes a numerosas outras drogas de segunda linha (5). Pacientes diagnosticados com XDR-TB possuem 64% mais chances de morrer durante o tratamento do que pacientes diagnosticados com MDR-TB. O alto grau de mortalidade destas cepas está intimamente associado à coinfecção pelo HIV, principalmente no continente africano e na Ásia.

Mais recentemente, identificou-se uma cepa XDR-TB na província de KwaZulu-Natal, na África do Sul, altamente mortífera, sendo que de 544 pacientes diagnosticados com TB na área em 2005, 221 apresentavam MDR-TB. Destes 221 pacientes, 53 foram diagnosticados com XDR-TB, sendo que o tempo médio de sobrevivência dos mesmos, a partir da coleta de amostras para exames, foi de 16 dias para 52 dos 53 pacientes, incluindo seis trabalhadores de saúde (6). Este panorama epidemiológico, associado ao fato de que há mais de quatro décadas não ocorre a introdução de novos agentes quimioterápicos para o tratamento da TB, criaram a necessidade urgente de desenvolvimento de novos medicamentos, que sejam menos tóxicos e que possam encurtar a duração do tratamento atual, além de sua produção em larga escala ser, economicamente, viável a países em desenvolvimento.

O desenvolvimento de novos agentes quimioterápicos para o tratamento da TB encontra vários obstáculos, sendo o principal deles o fraco interesse de grandes indústrias farmacêuticas em produzir medicamentos para este tipo de doença. Isso é explicado pelo fato de que mais de 95% dos casos de TB se localizam em países em desenvolvimento, principalmente na África e na Ásia e, portanto, o retorno financeiro não seria compensador frente ao tempo e os custos de desenvolvimento de um novo fármaco; estima-se que este processo consuma cerca de 15 a 20 anos e entre U$500-2000 milhões (7). Apesar de nos últimos 25 anos o investimento

governamental em programas de pesquisa e desenvolvimento de candidatos a drogas anti-TB ter aumentado, em especial o de importantes financiadores como o NIH (Institutos Nacionais de Saúde), nos EUA, eles ainda são insuficientes frente à ameaça à saúde global que a TB representa, com a ocorrência de mais de 2 milhões de mortes por ano, mundialmente. No período de 2001-2002, foram investidos U$ 2,049 bilhões em pesquisas com o HIV, contra U$ 378 milhões em TB (8).

No entanto, evidencia-se uma capacidade cada vez maior de propor inovações em saúde em países em desenvolvimento que possuem capacidade científica e tecnológica, mas força econômica relativamente baixa, nos quais estão incluídos Índia, China, Brasil, África do Sul, Tailândia, Argentina, Malásia, México e Indonésia. Coletivamente, estes países investem mais de U$ 2,5 bilhões por ano em pesquisas na área da saúde. Foi proposto que eles devam assumir uma posição de liderança na criação de inovações em saúde e que tenham como alvo, por exemplo, as doenças negligenciadas, como a TB e a malária, pois a maioria das pessoas que necessita de medicamentos mais efetivos se localiza justamente nestes países (9).

Como demonstrado acima, o desenvolvimento de novos agentes anti-TB é urgente. O desenvolvimento de novos análogos estruturais da INH parece representar uma abordagem promissora, frente ao perfil toxicológico favorável e à boa disponibilidade oral desta droga de primeira linha. Além do mais, a enzima InhA se apresenta como um alvo validado e inibidores de sua atividade podem prover uma rota mais rápida para o desenvolvimento de novas drogas. O composto pentaciano(INH)ferrato II, descrito neste trabalho, demonstra ser um candidato promissor para o futuro desenvolvimento de novas drogas anti-TB e representa uma nova classe de compostos líderes. Este composto possui perfis toxicológicos e microbiológicos favoráveis, apresentando um índice de seletividade >125 e uma concentração inibitória mínima de 0,2 μg mL^{-1}, comparável à determinada para a

INH, que varia de 0,02-0,2 μg mL^{-1} e sua dose tóxica em roedores é de 800 mg por Kg de peso, enquanto que a INH possui uma dose tóxica de 150 mg por Kg (10). Além do mais, este composto, ao contrário da INH, não necessita da presença de NADH e de ativação pela enzima micobacteriana KatG - mutações nesta enzima que ativa a INH são responsáveis por mais de 50% dos casos de resistência clínica a esta droga. Este composto também demonstrou ser um inibidor do tipo ligação lenta da enzima InhA espécie selvagem, possuindo uma constante global de inibição na ordem de 86 nM (11). A faixa mínima que um composto deve possuir para prosseguir no processo de desenvolvimento farmacêutico varia na faixa de 1-10 μM.

No presente trabalho, demonstrou-se através de um método simples e direto, que necessita apenas das enzimas e do inibidor em solução, o processo de ligação do inibidor pentaciano(INH)ferrato II às enzimas InhA espécie selvagem e mutantes resistentes à INH, através de técnicas de espectrofluorimetria. Além de demonstrar que o inibidor se liga às enzimas mutantes com eficácia semelhante à enzima selvagem, novos dados foram obtidos para sustentar a hipótese de que este inibidor segue um mecanismo de ação do tipo ligação lenta. O seu processo de ligação caracteriza-se por uma alteração gradual da fluorescência intrínseca dos aminoácidos triptofanos da proteína, condizente com a proposta de que a fase lenta de ligação ocorre devido a uma mudança conformacional no sítio ativo da enzima ou a um processo de isomerização da mesma.

Através da análise dos gráficos de velocidade contra a concentração de inibidor, tornou-se possível inferir que o mecanismo de inibição corresponde ao mecanismo B, descrito por Morrison e Walsh (12). Neste tipo de mecanismo ocorre, inicialmente, a formação de um complexo instável e reversível EI entre a enzima e o inibidor e, após, ocorre a lenta formação de um complexo final EI^{*}, onde o inibidor encontra-se mais fortemente ligado ao sítio ativo da enzima. Também demonstrou-

se, através de experimentos de recuperação da atividade enzimática, que o processo de isomerização reversa é lento para as enzimas mutantes, possuindo um tempo de meia-vida entre 7-9 horas. O principal problema do uso clínico de inibidores enzimáticos clássicos é que o processo inibitório conduz a um acúmulo de substratos, que em concentrações saturantes, podem ocasionar a reversão da inibição (EI $\rightarrow$E+I), tornando a enzima disponível para catalisar a reação novamente. Em inibidores do tipo ligação lenta, o acúmulo de substratos não conduz diretamente a este processo, pois o processo de reversão da isomerização é muito lento, na faixa de horas, como demonstrado neste trabalho. Este fator pode conduzir à necessidade de um maior intervalo entre as doses de um futuro medicamento e também a uma menor dose necessária para se atingir efeitos satisfatórios. Além disso, a constante de inibição global do composto (Ki^*) determinado para as enzimas mutantes (205, 263 e 303 nM para, respectivamente, S94A, I21V e I47T InhA) são muito semelhantes ao valor determinado para a espécie selvagem (225 nM), demonstrando que o composto inorgânico é eficaz em inibir as enzimas mutantes resistentes à INH.

Futuramente, será determinada a eficácia do composto em inibir o crescimento de cepas de *M.tuberculosis* resistentes às drogas, incluindo-se cepas que possuam mutações no gene *katG*, no gene *inhA* (incluindo-se as mutações pontuais S94A e I21V), além de cepas provenientes de isolados clínicos que sejam classificados como MDR-TB. A determinação da concentração inibitória mínima será realizada em um laboratório de nível de biosegurança 3 (NB3), disponível no Centro de Pesquisas em Biologia Molecular e Funcional – TecnoPUC, utilizando o método Alamar Blue em microplacas (13). Adicionalmente, será testada a capacidade do composto em inibir o crescimento de cepas virulentas de *M.tuberculosis* em modelos animais,

utilizando-se camundongos e também a sua capacidade de penetrar em macrófagos *in vitro*, através de cultura de células.

O composto inorgânico apresentado neste trabalho representa uma nova classe de compostos líderes promissores para o desenvolvimento de novas drogas anti-TB, que visa a inibição de um alvo molecular validado, possui bons perfis toxicológicos e microbiológicos, além de ser estável em pH ácido, podendo então ser usado futuramente como um medicamento por via oral.

4. Referências Bibliográficas

(1) World Health Organization. Global Tuberculosis Control Report, **2006.** Disponível em: www.who.int

(2) Center for Disease Control and Prevention. Emergence of *Mycobacterium tuberculosis* with extensive resistance to second-line drugs – worldwide, 2000-2004. Morb Mortal Wkly Rep. 2006;55:301-5.

(3) Shah NS, Wright A, Bai GH, Barrera L, Boulahbal F, Martín-Casabona N, et al. Worldwide emergence of extensively drug-resistant tuberculosis. Emerg Infect Dis. 2007;13:380-7.

(4) Centers for Disease Control and Prevention. Revised definition of extensively drug-resistant tuberculosis. Morb Mort Wkly Rep. 2006;55:1176.

(5) Hamilton CD, Sterling TR, Blumberg HM, Leonard M, McAuley J, Schlossberg D, et al. Extensively drug-resistant tuberculosis: are we learning from history or repeating it? Clin Infec Dis. 2007;45:338-42.

(6) Singh JA, Upshur R, Padayatchi N. XDR-TB in South Africa: no time for denial or complacency. PLoS Med. 2007;4(1):19-25.

(7) Adams CP, Brantner VV. Estimating the cost of new drug development: is it really $802 million? Health Aff. 2006;25(2):420-28.

(8) Kaufmann SHE, Parida SK. Changing funding patterns in tuberculosis. Nat Med. 2007;13(3):299-303.

(9) Morel CM, Acharya T, Broun D, Dangi A, Elias C, Ganguly NK, et al. Health innovation networks to help developing countries address neglected diseases. Science. 2005;309:401-04.

(10) Oliveira JS, Sousa EHS, Basso LA, Palaci M, Dietze R, Santos DS, et al. An inorganic complex that inhibits wild-type and an isoniazid-resistant mutant 2-*trans*-enoyl-ACP(CoA) reductase from *Mycobacterium tuberculosis*. Chem Commun. 2004;3:312-13.

(11) Oliveira JS, Sousa EHS, Souza ON, Moreira IS, Santos DS, Basso LA. Slow-onset inhibition of 2-*trans*-enoyl-ACP(CoA) reductase from *Mycobacterium tuberculosis* by an inorganic complex. Curr Pharm Des. 2006;12(19):2409-24.

(12) Morrison JF, Walsh CT. The behavior and significance of slow-binding enzyme inhibitors. Adv Enzymol Relat Areas Mol Biol. 1988;61:201-301.

(13) Franzblau SG, Witzig RS, McLaughlin JC, Torres P, Madico G, Hernandez A, et al. Rapid, low-technology MIC determination with clinical *Mycobacterium tuberculosis* isolates by using the microplate Alamar Blue assay. J Clin Microbiol. 1998;36(2):362-66.

5. Anexos – Outros artigos publicados durante o mestrado e iniciação científica

5.1. Phosphate closes the solution structure of the 5-enolpyruvylshikimate-3-phosphate synthase (EPSPS) from *Mycobacterium tuberculosis*. Arch Biochem Biophys. 2006;452(2):156-64.

Available online at www.sciencedirect.com
ScienceDirect
Archives of Biochemistry and Biophysics 452 (2006) 156–164
ABB
www.elsevier.com/locate/yabbi

Phosphate closes the solution structure of the 5-enolpyruvylshikimate-3-phosphate synthase (EPSPS) from *Mycobacterium tuberculosis*

Júlio C. Borges [a], José H. Pereira [a], Igor B. Vasconcelos [e], Giovanni C. dos Santos [a], Johnny R. Olivieri [a], Carlos H.I. Ramos [c], Mário S. Palma [d], Luiz A. Basso [b], Diógenes S. Santos [e,*], Walter F. de Azevedo Jr. [b,*]

[a] *Departamento de Física, UNESP, São José do Rio Preto, SP 15054-000, Brazil*
[b] *Faculdade de Biociências—Pontifícia Universidade Católica do Rio Grande do Sul, Porto Alegre, RS 90619-900, Brazil*
[c] *Laboratório Nacional de Luz Síncrotron, Campinas, SP 13084-971, Brazil*
[d] *Laboratório de Biologia Estrutural e Zooquímica, Departamento de Biologia, Instituto de Biociências, UNESP, Rio Claro, SP 13506-900, Brazil*
[e] *Centro de Pesquisas em Biologia Molecular e Funcional/PUCRS, Avenida Ipiranga 6681, Tecnopuc, Partenon 90619-900, Porto Alegre, RS, Brazil*

Received 31 January 2006, and in revised form 24 April 2006
Available online 13 June 2006

Abstract

The 5-enolpyruvylshikimate-3-phosphate synthase catalyses the sixth step of the shikimate pathway that is responsible for synthesizing aromatic compounds and is absent in mammals, which makes it a potential target for drugs development against microbial diseases. Here, we report the phosphate binding effects at the structure of the 5-enolpyruvylshikimate-3-phosphate synthase from *Mycobacterium tuberculosis*. This enzyme is formed by two similar domains that close on each other induced by ligand binding, showing the occurrence of a large conformation change. We have monitored the phosphate binding effects using analytical ultracentrifugation, small angle X-ray scattering and, circular dichroism techniques. The low resolution results showed that the enzyme in the presence of phosphate clearly presented a more compact structure. Thermal-induced unfolding experiments followed by circular dichroism suggested that phosphate rigidified the enzyme. Summarizing, these data suggested that the phosphate itself is able to induce conformational change resulting in the closure movement in the *M. tuberculosis* 5-enolpyruvylshikimate-3-phosphate synthase.

Keywords: Analytical ultracentrifugation; Circular dichroism; EPSPS; *Mycobacterium tuberculosis*; Shikimate pathway; Small angle X-ray scattering

Enzymes that form the shikimate pathway are attractive targets for development of non-toxic anti-microbial [1] and herbicides agents [2], since this pathway is essential for algae, higher plants, bacteria, and fungi, whereas it is absent in mammals [3]. Thus, in the case of bacterial diseases, inhibition of any enzyme responsible for the shikimate synthesis is unlikely to cause large toxic side effects on the host. The shikimate pathway links the metabolism of carbohydrates to the biosynthesis of aromatic compounds through seven metabolic steps, where phosphoenolpyruvate (PEP)[1] and

* Corresponding authors. Fax: +55 51 3320 3629 (W.F. de Azevedo Jr.).
E-mail addresses: diogenes@pucrs.br (D.S. Santos), walter.junior@pucrs.br (W.F. de Azevedo Jr.).

[1] *Abbreviations used:* AUC, analytical ultracentrifugation; CC, correlation coefficient; CD, circular dichroism; D, diffusion coefficient; $D_{20,w}$, standard diffusion coefficient; D_{max}, maximum distance; EPSP, 5-enolpyruvylshikimate-3-phosphate; EPSPS, EPSP synthase; *Mt*EPSPS, EPSPS from *Mycobacterium tuberculosis*; *Ec*EPSPS, EPSPS from *Escherichia coli*; *Sp*EPSPS, EPSPS from *Streptococcus pneumoniae*; GLP, glyphosate; PEP, phosphoenolpyruvate; Pi, phosphate; $p(r)$, distance distribution function; s, sedimentation coefficient; s^*, apparent sedimentation coefficient; $s_{20,w}$, standard sedimentation coefficient; $s^0_{20,w}$, standard sedimentation coefficient at 0 mg/mL of protein; S3P, shikimate 3-phosphate; SAXS, small angle X-ray scattering; R_g, radius of gyration; T_m, temperature at the midpoint transition; $[\Theta]$, residual molar ellipticity.

0003-9861/$ - see front matter © 2006 Elsevier Inc. All rights reserved.
doi:10.1016/j.abb.2006.05.008

erythrose 4-phosphate are converted into chorismic acid [4,5]. Chorismic acid is the common precursor for the synthesis of aromatic compounds, such as aromatic amino acids, pholate and ubiquinone, among others. The importance of shikimate pathway can be exemplified by observing that the deletion of the aroA gene, which codes 5-enolpyruvylshikimate-3-phosphate synthase, attenuates the virulence of *Streptomyces pneumoniae* and *Bordetella bronchiseptica* strains [6,7]. Another example that shows the importance of the shikimate pathway is that the EPSPS is the site of action of the *N*-[phosphomethyl]glycine, also known as glyphosate (GLP). It is the broad-spectrum active-compound of the non-selective herbicide RoundUp [8].

EPSPS is the sixth enzyme in the shikimate pathway, transferring the enolpyruvyl group from PEP to shikimate 3-phosphate (S3P) in order to form 5-enolpyruvyl-shikimate-3-phosphate (EPSP) and phosphate (P_i) [3,8,9]. The reaction depends on the order of substrate binding, which S3P binds first, followed by PEP, then releasing EPSP and P_i. The EPSPS reaction mechanism seems to involve a tetrahedral intermediary [9,10] that would be mimicked by the GLP compound [9]. The EPSPS crystallographic structures either free or bound to ligands (S3P, PEP analogues, and GLP–PDB access codes: 1Q36 [9]; 1RF4, 1RF5, and 1RF6 [10]; 1G6S and 1G6T [11]; 1EPS [12]; 1MI4 [13]), show that the enzyme suffered an extensive conformation change, which leads it to a closed state [9–13]. The *Ec*EPSPS and *Sp*EPSPS crystallographic structures show that the EPSPS closing, induced by ligands, occurs by a twist of one domain in relation to another, which imbeds the ligands between the domains and increases the enzyme rigidity [10,11]. Data from EPSPS in solution also points out this closing mechanism [14,15]. The EPSPSs are formed by two similar domains that possess six motifs for secondary structure type βαβαββ. These motifs are arranged so that their electronegative macrodipoles in the domain interface generate an attraction for anionic ligands [8,10,12]. The inhibitor GLP would compete with PEP for the binding site [11], but it also seems to involve an allosteric component, as suggested by Sikorski and Gruys [16] and Du et al. [17]. Despite the high conservation on the secondary/tertiary structure [9–13], EPSPS proteins present low conservation on the amino acid sequence which would imply in differences on the action mechanism and/or affinity for ligands [10].

Our group has dedicated efforts to study the 5-enolpyruvylshikimate-3-phosphate synthase (EPSPS—EC 2.5.1.19) from *Mycobacterium tuberculosis* (*Mt*EPSPS), which resulted in the enzyme production and activity characterization [18,19], including the protein structure modeling [20]. We have been studying the ligand effects on the *Mt*EPSPS structure by low resolution techniques, like analytical ultracentrifugation (AUC), small angle X-ray scattering (SAXS) and, circular dichroism (CD), aiming to improve the overall knowledge about *Mt*EPSPS. Here, we report *Mt*EPSPS studies in equilibrium conditions with P_i, an EPSPS reaction product, which binds weakly to EPSPS complexes [14]. Our results suggested that *Mt*EPSPS, in the presence of P_i, was in its closed conformation, and it was in the open state in the absence of P_i. To our knowledge, this is the first report showing that P_i alone fixes an EPSPS in the closed conformation.

Materials and methods

Protein sample

The active recombinant *Mt*EPSPS was expressed and purified as previously described [18,19]. The pellet from this protein saturated with ammonium sulphate 80% was resolubilized and dialyzed exhaustively against either Tris–HCl 50 mM (pH 7.6) or sodium/potassium phosphate (Na/K P_i) 100 mM (pH 6.8) buffers. The protein concentration was determined spectrophotometrically, using the calculated extinction coefficient for native conditions or for denatured proteins [21].

Hydrodynamic characterization

The diffusion coefficients (D) were obtained by dynamic light scattering using a DynaPro-MS/X device (Protein Solutions) at 20 °C and in the two *Mt*EPSPS conditions described above. The software Sednterp (www.jphilo.mailway.com/download.htm) was used to estimate the following *Mt*EPSPS properties: partial specific volume ($V_{bar} = 0.7361$ mL/g), the buffers viscosity (ηNa/K $P_i = 1.0474 \times 10^{-2}$ poise and ηTris–HCl $= 1.0167 \times 10^{-2}$ poise), density (ρNa/K $P_i = 1.01263$ g/mL and ρTris–HCl $= 0.99966$ g/mL), and D_{sphere} for a globular protein of about 46 kDa. The HydroPro software [22] was applied to estimate the standard diffusion coefficient ($D_{20,w}$) and the maximum distance (D_{max}) from the *Mt*EPSPS models previously developed [20].

AUC experiments were performed with a Beckman Optima XL-A analytical ultracentrifuge. The *Mt*EPSPS was tested in concentrations of 50, 100, and 200 μg/mL in either Tris–HCl or Na/K P_i buffers. The sedimentation velocity experiments were carried out at 20 °C, 40,000 rpm (AN-60Ti rotor), and the scan data acquisition was taken at 225 nm. The software SedFit (Version 9.3) was used in order to fit the absorbance versus cell radius data. This software solves the Lamm equation so as to discriminate the spreading of the sedimentation boundary from diffusion [23,24]. Thus, we used the D estimated by the dynamic light scattering experiments to calculate the high resolution sedimentation coefficient distributions $c(s)$. The maximum of Gaussian curves of the $c(s)$ resulted in the apparent sedimentation coefficient s^*. The ratio of the sedimentation coefficient (s) to diffusion coefficient (s/D ratio) gives the molecular mass as indicated by Eq. (1):

$$M = \frac{sRT}{D(1 - V_{bar}\rho)} \quad (1)$$

where R is the gas constant and T is the absolute temperature. The Sednterp software was used to estimate the standard sedimentation coefficients ($s_{20,w}$) at each protein concentration from the s^* in order to calculate, by extrapolation, the $s^0_{20,w}$, at 0 mg/mL of protein concentration. This procedure minimizes interferences caused by temperature, viscosity, and molecular crowd [25]. The HydroPro software [22] was applied to estimate the $s_{20,w}$ from the M*t*EPSPS models [20].

Circular dichroism spectroscopy

Circular dichroism (CD) measurements were performed in a Jasco J-810 spectropolarimeter with the temperature controlled by a Peltier-type control system PFD 425S. The *Mt*EPSPS protein was tested in either Tris–HCl or Na/K P_i buffers at final concentrations of 200–2000 μg/mL. The spectra were collected at a scanning rate of 100 nm/min with a spectral band width of 1 nm and using a 0.1 mm pathlength cell. The resultant spectra were normalized to residual molar ellipticity ($[\Theta]$) and the software CDNN Deconvolution [26] was used for estimating the *Mt*EPSPS secondary structure content. The thermal-induced unfolding experiments followed by CD were performed at a temperature rate of 1 °C/min and a protein concentration of 200 μg/mL in the conditions above described, using a 1 mm pathlength cell. The average of three unfolding curves was used to build the *Mt*EPSPS thermal-unfold profile, and the temperature at the midpoint of each unfolding transition (T_m) was determined by fitting with Gaussians curves (one or two) of the first derivative function.

SAXS studies

X-ray scattering data were collected at room temperature using CuKα X-rays radiation generated by a Rigaku RU300 rotating anode generator operated at 50 kV and 90 mA and collimated with a block slit system [27]. The scattering intensity was measured using a linear position sensitive detector (CBPF-Brazil). The SAXS measurements were performed within an angular range defined by $0.02\ \text{Å}^{-1} < h < 0.450\ \text{Å}^{-1}$: $h = (4\pi \sin 2\theta)/\lambda$, 2θ is the angle between the incident and the scattered X-ray beam, and λ is the X-ray wavelength. The contributions to the scattering intensity from the solvent, capillary, and air were subtracted from the total intensity. *Mt*EPSPS SAXS measurements were carried out at a concentration of 12 mg/mL in Na/K P_i buffer and also in Tris–HCl buffer. The measurement time was of 12 h. The experimental SAXS intensity function was desmeared to suppress the influence from the slit collimation system yielding the corrected intensities, $i(h)$.

A structural parameter related to the overall size of macromolecules, the radius of gyration (R_g), was determined by the Guinier equation [28]:

$$I(h) = I(0)e\left[\frac{-h^2R_g^2}{3}\right] \tag{2}$$

This equation applies to macromolecules in the limits of a diluted solution and small h values. More detailed information of the molecular structure can be obtained from the distance distribution function ($p(r)$), which is related to the SAXS intensity $i(h)$ by:

$$p(r) = \frac{1}{2\pi^2}\int_0^\infty (rh)I(h)\text{sen}(rh)\text{d}h \tag{3}$$

The $p(r)$ curve is proportional to the number of pairs of electrons separated by the distance r, which is encountered by combinations between all the elements of the macromolecule. The R_g of macromolecules in solution is usually determined by applying Eq. (2) or alternatively through $p(r)$ function using the Eq. (4).

$$R_g^2 = \frac{\int_0^\infty p(r)r^2\text{d}r}{2\int_0^\infty p(r)\text{d}r} \tag{4}$$

The experimental distance distribution function, $p(r)_{exp}$, has been determined by indirect Fourier transformation using the ITP program [27]. This software was also employed to determine the intensity $i(h)$, which was free from smearing collimation effects. The theoretical $p(r)_{theo}$ function of the protein models was calculated by the program MULTIBODY [27], modified in order to make molecular model building easier [29]. The program MULTIBODY calculates the resulting function $p(r)$ of the complete set of atomic coordinates of each structural model for the macromolecule. In the present study we calculated the $p(r)_{theo}$ for the open and the closed *Mt*EPSPS models previously developed [20]. To assess the correlation between theoretical and experimental distance distribution function $p(r)_{exp}$ and $p(r)_{theo}$, respectively, we have calculated the linear correlation coefficient (CC) [30], as previously showed by De Azevedo et al. [31]. Briefly, when a correlation is known to be significant, CC is a conventional way of summarizing its strength. The shape, which generates the highest CC, is considered the greatest macromolecular conformation.

Results and discussion

*Mt*EPSPS shares, in the amino acid sequence, 30% and 20% of identity with the enzymes from *Escherichia coli* and *S. pneumoniae*, respectively, which have their crystallographic structures available from PDB (1Q36 [9]; 1RF4, 1RF5, and 1RF6 [10]; 1G6S and 1G6T [11]; 1EPS [12]; 1MI4 [13]). This low conservation would imply differences on the action and regulation mechanism for the *Mt*EPSPS in comparison to the other enzymes. For instance, differences in the affinity from a range of 10–200 times between EPSPS and GLP on several organisms have been reported [32]. Slight differences on the closing mechanism have also been reported: the twist of one domain against another, in the *Ec*EPSPS, is of about 65°, whereas it is around 30° in the *Sp*EPSPS [10]. These data justify the necessity of the evaluation of the ligand biding effects on EPSPS from

several sources in order to determinate their action mechanism, which may be helpful on future inhibitor development. In this report, we present results of the effect of P_i on the *Mt*EPSPS structure, which is an EPSPS reaction product [16] and is able to induce conformational changes on the *Ec*EPSPS structure [14]. For this study we used *Mt*EPSPS samples prepared by exhaustive dialysis in both presence of P_i dianion (Na/K P_i buffer) and in its absence (Tris–HCl buffer).

Sample quality

First, in order to verify the quality of our *Mt*EPSPS sample in the two conditions, the Tris–HCl and in the Na/K P_i buffers, we performed dynamic light scattering experiment in protein concentration ranging from 0.5 to 3.5 mg/mL. The *Mt*EPSPS samples behaved as a monodispersive solution in either Tris–HCl or in Na/K P_i buffers, and the $D_{20,w}$ estimated for the protein was of about 7.1 and 7.6×10^{-7} cm^2/seg, respectively. These results were similar to those values calculated by the HydroPro software to open and closed *Mt*EPSPS models (Table 1). The $D_{20,w}$ values obtained are in accordance with particles presenting molecular mass of around 50–60 kDa.

The CD technique was used in order to characterize the *Mt*EPSPS secondary structure content in the Tris–HCl buffer and also in the Na/K P_i buffer. Fig. 1 represents the *Mt*EPSPS CD spectra in both conditions, showing that they were similar and that the protein presented α-helices as its main secondary structure content. These data were consistent with the CD spectra for the *Sp*EPSPS, showing that the presence of several ligands does not change the CD spectra [17]. The secondary structure content estimated by the CDNN Deconvolution software [26] in the two conditions was: 32% in α-helix, 19% in β-sheet, 17% in turns, and 31% in coils (error was less than 5%). The *Ec*EPSPS and *Sp*EPSPS crystallographic structures deposited in the Protein Data Bank have similar secondary structure content: 30% in α-helix and 23% in β-sheet (PDB access codes: 1Q36 [9]; 1RF4, 1RF5 and 1RF6 [10]; 1G6S and 1G6T [11]; 1MI4 [13]). The secondary structure content of the *Mt*EPSPS models [20] were analyzed by the Procheck software [33], and estimated at 31% in α-helix and 25% in β-sheet, showing a similar result to the experimental data. Altogether, the dynamic light scattering and CD experiments attested the *Mt*EPSPS structural integrity and quality in both Tris–HCl and in Na/K P_i buffers.

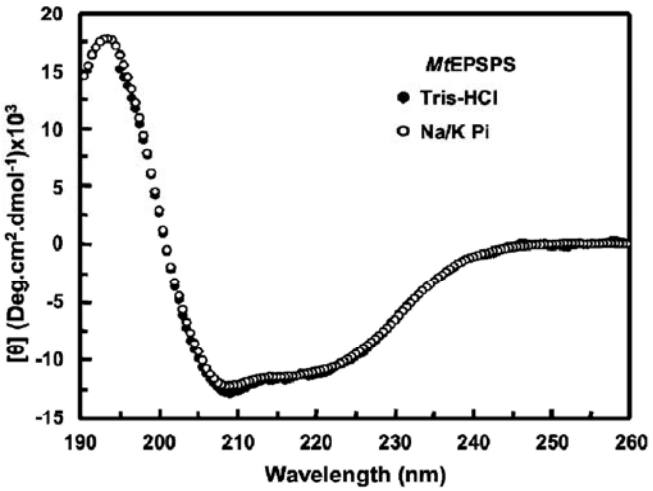

Fig. 1. *Mt*EPSPS presents high α-helix content. Residual molar ellipticity [θ] of *Mt*EPSPS were measured from 190 to 260 nm in Tris–HCl and Na/K P_i buffers at 20 °C and in a 0.1 mm pathlength cell. The amount of secondary structures to *Mt*EPSPS were calculated by CDNN Deconvolution software and the results was: 32% in α-helix, 19% in β-sheet, 17% in turns, and 31% in coils (error was less than 5%).

AUC experiments

Sedimentation velocity experiments were carried out in the presence and the absence of P_i (Na/K P_i and Tris–HCl buffer, respectively), in order to obtain information about the shape of the *Mt*EPSPS. Fig. 2 shows the sedimentation coefficient distribution $c(s)$ of the *Mt*EPSPS in the two conditions, where the maximum of the Gaussian curves gives the s^*. In order to avoid interferences caused by the solution viscosity and molecular crowd [25], we determined the $s^0_{20,w}$ (Fig. 2, inset and Table 1). The results of the sedimentation velocity experiments showed that the *Mt*EPSPS samples behaved as a monodispersive solution and that the molecular mass estimated by the ratio of the s/D (Eq. (1)) was of around 44 ± 1 kDa in either buffers. This value is nearly of the calculated from the *Mt*EPSPS amino acid sequence, showing that the *Mt*EPSPS was monomeric in the conditions tested. The $s^0_{20,w}$ estimated for the *Mt*EPSPS, as the one estimated for the $D_{20,w}$, (Table 1) evidenced that the protein presented an asymmet-

Table 1
Structural and hydrodynamic parameters derived from the SAXS and DLS data and estimated to the *Mt*EPSPS models by the HydroPro Software

*Mt*EPSPS	$D_{20,w}$ ($10^{-7}$$cm^2$/seg)	$s^0_{20,w}$ (S)	D_{max} (Å)	R_g (Å)		CC
				Guinier plot	$p(r)$	
Na/K P_i	7.6 ± 0.1	3.48 ± 0.05	61 ± 2	22.2 ± 0.6	22.0 ± 0.6	0.9954[$]
Closed model[a]	7.5 ± 0.1	3.68 ± 0.05	62 ± 3	—	21.8 ± 0.2	
Tris–HCl	7.1 ± 0.1	3.32 ± 0.01	72 ± 2	23.8 ± 0.7	24.8 ± 0.7	0.9653[&]
Open model[a]	6.9 ± 0.1	3.39 ± 0.04	75 ± 3	—	24.9 ± 0.3	

$ and & are the CC between the $p(r)$ curves from the SAXS data and the predicted from the closed and open *Mt*EPEPS models, respectively.
[a] Data estimated by the HydroPro Software.

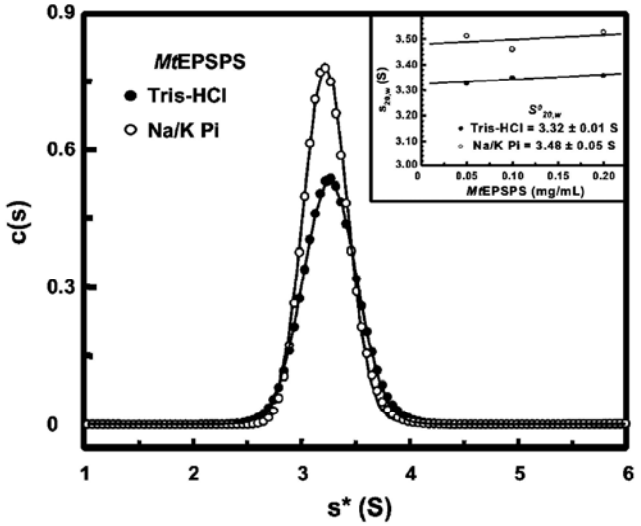

Fig. 2. AUC experiments show that *Mt*EPSPS was more globular in the presence of P_i than in its absence. Sedimentation velocity experiments were carried out at 20 °C, with rotor (AN-60Ti) at the velocity of 40,000 rpm. The figure displays experiments with 50 μg/mL of the *Mt*EPSPS in both Tris–HCl and Na/K P_i buffers. The $c(s)$ distributions were fitted using the SedFit software [23,24] and the maximum of Gaussian curves resulted in the apparent sedimentation coefficient s^*. The D estimated for the protein in either conditions was used in the fitting routine. Inset: plots of $s_{20,w}$ versus protein concentrations were fitted by linear regression to calculate the $s^0_{20,w}$ (Table 1). The software Sednterp was used for the correction of the s^* to the $s_{20,w}$, eliminating the effects of viscosity and molecular crowd [25].

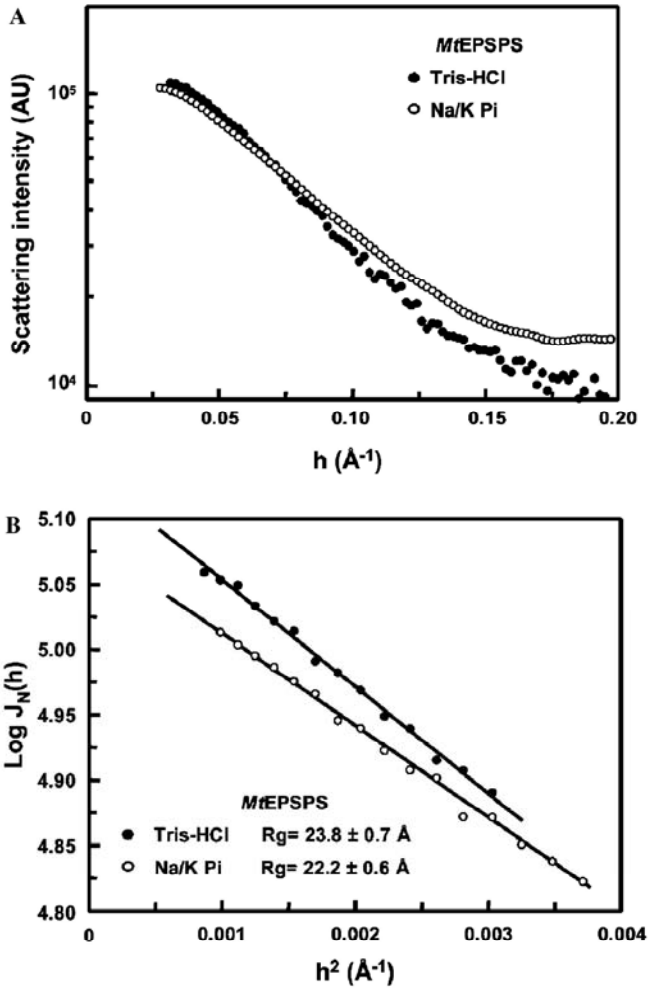

Fig. 3. Experimental SAXS curves of *Mt*EPSPS. The *Mt*EPSPS SAXS experiments were carried out with a protein concentration of 12 mg/mL in the Tris–HCl and in the Na/K P_i buffers (see Materials and methods for details). (A) Plot of log$I$ versus h (logarithmic scale) focusing on the features of SAXS curves at high h. (B) Guinier plot (log$I$ versus $h2$) within the small h range, showing the good data quality. The values of the *Mt*EPSPS R_g, derived from Guinier plot, can be found in Table 1.

ric shape. Both the s_{sphere} and D_{sphere} for a spherical particle of 46,426 Da (*Mt*EPSPS' molecular mass) were estimated by the software Sednterp at about 4.5 S and 8.9×10^{-7} cm^2/seg, consecutively. These data suggest that the *Mt*EPSPS had a frictional ratio of about 1.3 (data not shown).

The AUC results also showed that the $s^0_{20,w}$ was slightly different in the presence of P_i when compared in its absence. In the Na/K P_i buffer, the *Mt*EPSPS presented a $s^0_{20,w}$ higher than in the Tris–HCl buffer: 3.48 ± 0.05 S versus 3.32 ± 0.01 S, respectively. These values were in agreement with the ones estimated by the HydroPro software for the *Mt*EPSPS models in either open or closed conformation (Table 1). Thus, these data suggested that the *Mt*EPSPS in presence of P_i ions was more globular or compact than in its absence, suggesting that the enzyme in presence of P_i was in the closed state (see below).

SAXS experiments

Fig. 3A shows the $i(h)$ curves derived from SAXS experiments for the *Mt*EPSPS in two buffer conditions, suggesting differences in the scattering particle. These differences may be best verified by the evaluation of the R_g, obtained from the Guinier plot (Fig. 3B), which is a fine tool to observe overall conformation changes on the molecule structure [34]. The R_g for the *Mt*EPSPS in the presence of P_i was of 22.2 ± 0.6 Å and in its absence was of 23.8 ± 0.7 Å. These data suggested that *Mt*EPSPS has distinct structures in those different chemical conditions. An overall reduction of the R_g of the *Ec*EPSPS is observed after the S3P and GLP binding, as had been examined by SAXS [35]. The $p(r)$ curves represent the same information contained in the $i(h)$ curves (Fig. 3A), but $p(r)$ curves possess a more discernable representation, supplying information about the size (D_{max}) and shape of the scattering particle from the direct inspection of its curve [34]. Figs. 4A and 5A show the $p(r)_{exp}$ curves from the *Mt*EPSPS in the Na/K P_i and Tris–HCl buffers, respectively. It is also possible to estimate the R_g from the $p(r)$ (see Materials and methods), and the values obtained for *Mt*EPSPS were similar to those determined by application of the Guinier plot (Table 1). These data were in accordance with our experimental results from AUC experiments, suggesting that P_i binding is responsible for changes on the *Mt*EPSPS structure.

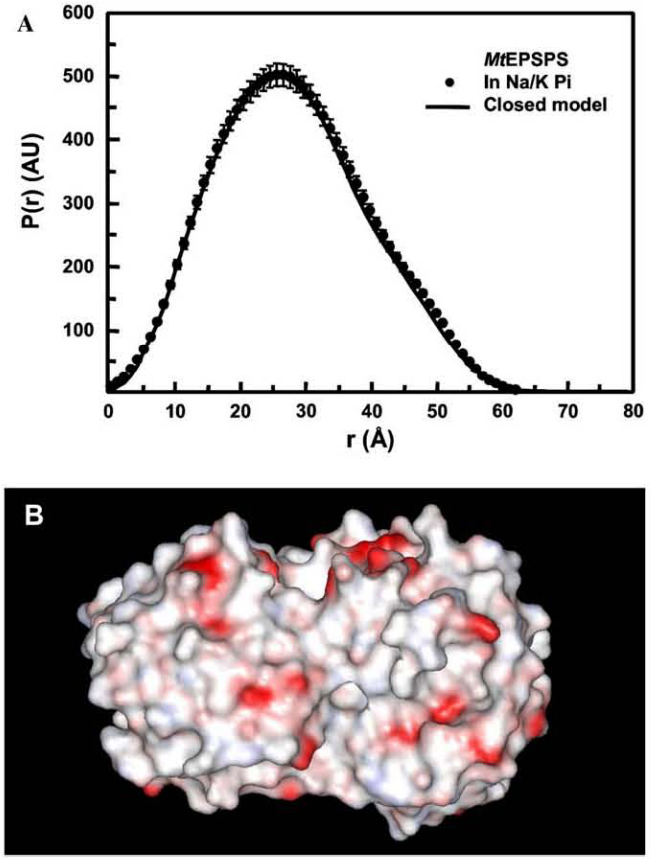

Fig. 4. *Mt*EPSPS distance distribution function in Na/K P_i buffer. (A) The $p(r)_{exp}$ curve of the *Mt*EPSPS in Na/K P_i buffer was calculated by indirect Fourier transformation using the ITP program. The $p(r)_{theo}$ from the *Mt*EPSPS closed model (represented in (B)), was calculated using the program MULTIBODY. The discrepancy between the $p(r)_{exp}$ and $p(r)_{theo}$, given by the CC value, was of about 0.9954, showing the good correlation of these two curves and suggesting that in the presence o P_i ions, the *Mt*EPSPS is in its closed conformation. The R_g and D_{max} of these curves are presented in Table 1.

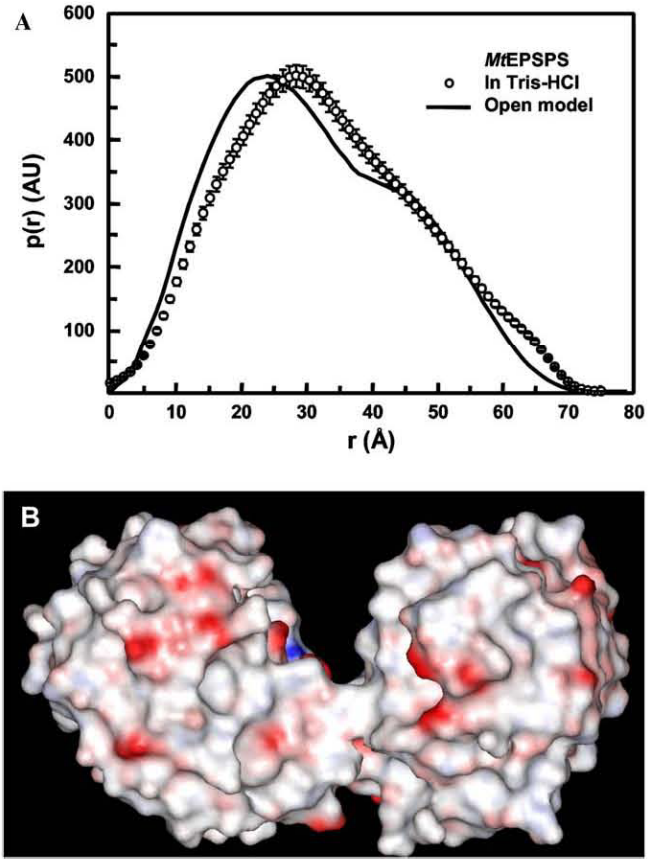

Fig. 5. *Mt*EPSPS distance distribution function in Tris HCl buffer. (A) The $p(r)_{exp}$ curve of the *Mt*EPSPS in Tris HCl buffer was calculated by indirect Fourier transformation using the ITP program. The $p(r)_{theo}$ from the *Mt*EPSPS open model (represented in (B) attention for the cleft between the two domains), was calculated using the program MULTIBODY. The discrepancy between the $p(r)_{exp}$ and $p(r)_{theo}$, give by the CC value, was of about 0.9653. Despite some parts of the $p(r)_{exp}$ and $p(r)_{theo}$ not showing a good fitting, there are a good correlation between the R_g and D_{max} of both curves (Table 1), indicating that they present some resemblance (see Results and discussion for details).

The $p(r)_{theo}$ curves were plotted for the *Mt*EPSPS closed and open models, and are also showed in Figs. 4A and 5A, respectively. These models are demonstrated, for comparison, in Figs. 4B and 5B, respectively. The correlation coefficient CC between the $p(r)_{exp}$ and $p(r)_{theo}$, as well as the values of the R_g and D_{max} (Table 1) estimated by the HydroPro software for the *Mt*EPSPS closed and open models, demonstrate that they are similar to those experimentally determined (see below). On the whole, the data suggested that the *Mt*EPSPS closed and open models are high-quality models for this protein in solution, either in presence of P_i or in its absence, respectively. Fig. 4A shows that the closed model fits well the experimental SAXS data in the presence of P_i, presenting a CC of about 0.9954 (Table 1). However, the *Mt*EPSPS open model did not fit quite well to the $p(r)_{exp}$ obtained from SAXS in Tris–HCl buffer (Fig. 5A), although the R_g and D_{max} were indeed in agreement (Table 1). Fig. 5A suggests that the $p(r)_{theo}$ from the *Mt*EPSPS open model presents a shape that resembles a particle that would be formed by a well-separated subunits or lobules, like a halter [34]. However, the $p(r)_{exp}$ from the *Mt*EPSPS in Tris–HCl resembled a prolate asymmetric protein, in which no clear globules were observed [34]. The explanation for this 'apparent contradiction' may be the flexibility and dynamics of the *Mt*EPSPS in the open conformation. Some authors have reported that the EPSPSs from other organisms are flexible and that their rigidity increase in the presence of ligands [10,11,15]. On the other hand, it is worth to mention that the SAXS technique supplies information about a "time averaged conformation", indicating the main conformation presented by the scattering particle [34]. Therefore, the discrepancy between the $p(r)_{exp}$ of the *Mt*EPSPS in the Tris–HCl buffer and the $p(r)_{theo}$ of the open model would suggest that its dynamic conformational equilibrium was dislocated to the open conformation. Moreover, the presence of P_i changed the *Mt*EPSPS conformation toward the closed state.

Thermal-unfolding experiments

Fig. 6 (upper panel) represents the thermal-induced unfolding experiments followed by CD. These data suggested that the *Mt*EPSPS initiated its thermal unfolding after 40 °C and that it was influenced by the buffer composition: the unfolding curve in the presence of P_i dianion occurred at higher temperatures than in its absence. The *Mt*EPSPS in the presence of P_i unfolded with a T_m at 56.4 °C, while in the Tris–HCl buffer it unfolded at 53.8 °C (Table 2). Analyzing the profile of the first derivative function of the *Mt*EPSPS thermal-induced unfolding curve (Fig. 6 – lower panel), we can notice shoulders in the curves, which interfered in their fitting by using one Gaussian function only (data not shown). Considering that the EPSPSs possess two domains of similar sizes and foldings [8,10,12], it would be expected alike thermal stability, as we observed for *Mt*EPSPS. Fitting the first derivative curves with two Gaussian system (data not shown); we can observe two close T_ms (Table 2). In the presence of Na/K P_i buffer, the T_ms estimated for both domains were 2-3 °C higher than the ones observed in the Tris–HCl buffer (Table 2). These data suggested that in the presence of P_i the *Mt*EPSPS presents more thermal stability than in its absence, which may be a consequence of an increased rigidity; as described for the closed conformation from EPSPSs in the presence of ligands [10,11,15]. Considering the two T_ms above described, we can conclude that the two *Mt*EPSPS domains were influenced by the presence of the P_i, suggesting an interaction of the dianion with both domains. Thus, the P_i binding site is possibly in the cleft between the domains. In all conditions tested, the *Mt*EPSPS thermal-unfolding was irreversible.

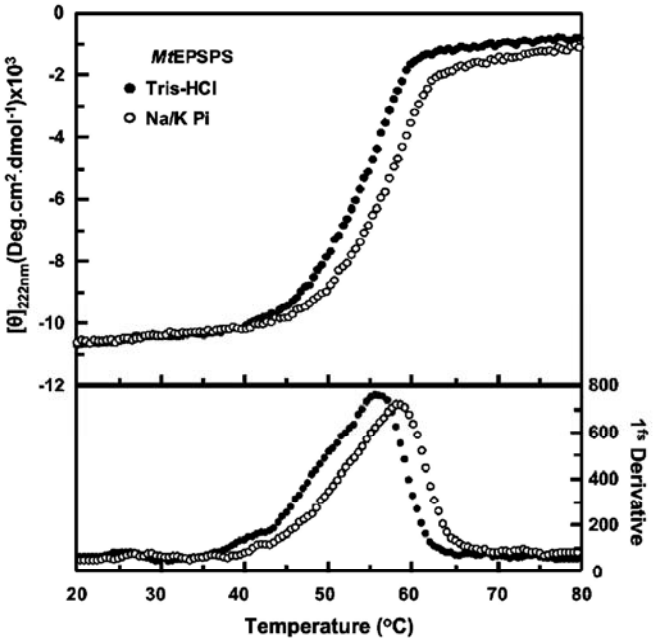

Fig. 6. *Mt*EPSPS thermal-induced unfolding experiments. *Mt*EPSPS (200 μg/mL) in the Tris–HCl or Na/K P_i buffer were submitted to a thermal-unfolding followed by CD at 222 nm. The unfolding experiments (in triplicate) were measured from 20 to 80 °C, irreversible though, showing a precipitation after the temperature decrease. The upper panel represents the three unfolding experiments average. The lower panel represents the first derivative of the temperature-unfolding curve that was used to be fitted by Gaussian curves, where the maximum of Gaussian curves resulted in the T_m (Table 2). The T_m was determined for each curve and represents the average of the three thermal-unfolding curves from fitting with 1, and 2 Gaussian systems (see text for details).

Table 2
Set of T_m determined from *Mt*EPSPS unfolding assays followed by CD

*Mt*EPSPS	Unfolding temperature (°C)		
	1 Gaussian	2 Gaussian	
	T_m	T_{m1}	T_{m2}
Tris–HCl	53.8 ± 0.3	51.6 ± 0.4	56.4 ± 0.2
Na/K P_i	56.4 ± 0.1	54.5 ± 0.6	58.6 ± 0.2

The first derivative of the *Mt*EPSPS unfolding profile were fitted by 1 Gaussian or 2 Gaussian systems (see Results and discussion for details).

MtEPSPS conformation remarks

In the previous sections, we presented results that attested the quality of the *Mt*EPSPS samples, showing that they were monomeric. They possessed an asymmetric shape, and the α-helix as its main secondary structure content. All these data are in accordance with the current knowledge about the EPSPS structure [9–13]. In either conditions tested, *Mt*EPSPS CD spectra were very similar to each other, suggesting that the conformational changes observed by AUC, SAXS, and thermal-induced unfolding experiments were mainly in the tertiary structure level. In fact, the superposition of the EPSPS domains in open and closed conformation showed that they possess similar secondary structure content (data not shown).

In this report, we used three independent tools in order to monitor the *Mt*EPSPS structure and the conformational change induced by P_i. The AUC is able to provide information about hydrodynamics properties of proteins and their shape in solution [25]. SAXS technique supplies data about the protein structure at low resolution in solution as well [34]. Thermal unfolding followed by CD may supply data about the thermodynamic interactions between proteins and ligands. Altogether, the AUC, SAXS, and thermal-unfolding results presented here suggested that in the presence of P_i, *Mt*EPSPS was in a more compact form than in the absence of this dianion. Such compacted structure resembled EPSPS in the closed state, as previously determined by crystallographic studies in the presence of ligands (PDB access codes: 1Q36 [9]; 1RF4 and 1RF6 [10]; 1G6S and 1G6T [11]; 1MI4 [13]).

Schönbrunn et al. [11] awoke to the sequence of ligands binding in which the first S3P binds to *Ec*EPSPS and that S3P itself would be able to close the enzyme. However, Alibhai and Stallings [8] suggest that another ligand might be important to the full EPSPS closure. Therefore, the P_i dianion and the formate ion should be considered, since

they have been found in the *Ec*EPSPS–S3P complex structure; occupying the GLP binding site (PDB access code 1G6T - [11]). These data suggest that P_i may be important for the full closure of the EPSPS–S3P complex. Moreover, thermodynamic and mass spectrometry data reports describe that S3P by itself is unable to induce the complete EPSPS closure. Thus, another ligand is needed, like PEP or GLP, to induce the full conformation change effect on the EPSPS structure [14,15,17]. That means the participation of many other ligands may be important for inducing full EPSPSs conformational changes, including P_i.

Park et al. [10] propose that the EPSPS domains, in the unbound state, present a "dynamic motion" that is in equilibrium between the open and closed conformations. Our SAXS results for *Mt*EPSPS in the Tris–HCl buffer, presented agreement with the R_g and D_{max} of the *Mt*EPSPS open model, but disagreed between the $p(r)_{theo}$ and the $p(r)_{exp}$ curves. This discrepancy would be according to the "dynamic motion" hypothesis above described, since SAXS data represent an average data time that shows the main conformation of the scattering particle [34]. Park et al. [10] suggests that S3P binding to EPSPS should disturb the equilibrium toward an incomplete closed conformation, when should be fully closed after the PEP or GLP binding. Additionally, the closure motion would imply an increment of the relative protein stability [10]. Regarding all these propositions, our results suggest that P_i should bind in the cleft and can shift the *Mt*EPSPS equilibrium toward a closed form, reducing its R_g, and making it more globular and increasing its thermal stability. The *Sp*EPSPS structure possesses a 'reversible gate' or channel on its structure that should allow the PEP (or GLP) entering to the binding site in the *Sp*EPSPS–S3P complex incompletely closed [10]. The PEP (or GLP) binding should be the ligand responsible for inducing the complete EPSPS closure. Thus, even when the conformation is partially closed, the binding of another ligand to *Mt*EPSPS–S3P (or another state) would happen.

Metallic ions have a significant effect on the activity of EPSPS from *Klebsiella pneumoniae* [36] and from *Pseudomonas aeruginosa* [37]. It has been demonstrated that *Sp*EPSPS was activated by univalent cations in the following order: $NH_4^+ > Rb^+ > K^+ > Na^+ > Cs^+ > Li^+$ [38]. Moreover, *Sp*EPSPS became increasingly more susceptible to inhibition by GLP when increasing NH_4^+ concentrations [38]. EPSPS from other species, including *E. coli*, are not activated by univalent cations. Du et al. [38] and Priestman et al. [32] showed that some monovalent cations are allosteric EPSPS activators, having the ammonium ion as the highest activator, and potassium as a moderate activator. As the used Na/K P_i buffer contains 100 mM of potassium, it could possibly influence the *Mt*EPSPS structure. Nevertheless our thermal-unfolding experiments in potassium absence (with 100 mM of Na_2 P_i buffer) presented the same profile as it was observed in the Na/K P_i buffer (data not shown), suggesting that potassium did not influence the *Mt*EPSPS structure and the effects observed were due to the presence of P_i. We illustrate three other evidences that imply the P_i in the *Mt*EPSPS conformational change is important. First, the P_i dianion is an EPSPS reaction product [3,16]. Second, P_i is found in the EPSPS binding site at the *Ec*EPSPS–S3P crystallographic structure [11]. And third, P_i is able to close on the *Ec*EPSPS–S3P preformed complex, as it is discussed below, even in the presence of potassium [14].

We did not find any report describing the association constant of any EPSPS for P_i, despite the thermodynamic data for the interaction of the *Ec*EPSPS with several ligands [14]. S3P binds to *Ec*EPSPS, but it is unable to induce the domains closure by itself, since the entropy energy variation of this interaction is positive. These data indicate that no high conformation change occurred on the protein structure, leading it to lose the flexibility or to a more compact form [14]. On the other hand, GLP binding to *Ec*EPSPS–S3P complex induces a high negative entropy variation, suggesting a huge conformation change accompanied by a protein organization with loss of flexibility. These data suggest that GLP is able to close on the *Ec*EPSPS [14]. Similar results are reported about the EPSPS from *S. pneumoniae* [17]. Analyzing the entropy energy variation, the data suggest clearly that the P_i is able to induce the closure motion of the *Ec*EPSPS–S3P preformed complex, like GLP is [14]. In our point of view, this information reinforces that the compact *Mt*EPSPS state described above is due to the P_i binding. P_i may possibly posses multiple binding sites in the EPSPS cleft; because of the many positive charges on their domains interface [12]. This fact may explain the difficulty in determinate the reaction stoichiometry between P_i and *Ec*EPSPS–S3P complexes in the isothermal titration calorimetric experiments performed by Ream et al. [14]. By analyzing the binding site in the crystallographic complex structures of *Sp*EPSPS and *Ec*EPSPS we have observed that the amino acids which interact with the P_i moiety are mainly localized in the N-terminal domain [9–11]. Considering that the S3P binding site is mainly on the N-terminal domain and that it could be able to dislocate the domain equilibrium to the closed conformation [10,11], hence we propose that P_i binding could also induce similar effects on the *Mt*EPSPS structure. P_i may interact with the *Mt*EPSPS N-terminal domain neutralizing the positive charges in the cleft interface allowing the domains to interact, leading to the protein closure.

Conclusion

In this work, we presented data from three independent tools indicating that P_i induced conformational change on the *Mt*EPSPS structure, leads it to a more compact shape resembling the EPSPSs closed state. The AUC data suggested that the protein in the presence of P_i was more globular than in its absence. The SAXS data clearly suggested that the *Mt*EPSPS in presence of P_i possesses a shape slightly different than in its absence, as analyzed by the

R_g, D_{max}, and $p(r)$ curve. Moreover, there was a high correlation coefficient between the experimental and the predicted $p(r)$ curve from the previously modeled *Mt*EPSPS in both closed and open conformation. The protein stability in the thermal-induced unfolding was shifted to higher temperatures in presence of P_i, suggesting that the *Mt*EPSPS structure was more rigid in this condition. Our results are also in accordance with the previously "dynamic domain motion" equilibrium described between the open and closed conformation, and that ligand binding leads the *Mt*EPSPS to the closed state. The results presented will be important in the EPSPS–ligand interaction mechanism context, for determining the P_i dianion importance for EPSPS closure and consequently in a drug development context [39].

Acknowledgments

This work was supported by grants from FAPESP (SMOLBNet, Proc. No. 00/01586-9, 01/07532-0, 02/05347-4, and 04/00217-0) and Millenium Institute, MCT/CNPq, PRONEX, FAPERGS to D.S.S. and L.A.B. W.F.A., M.S.P., C.H.I.R., L.A.B., and D.S.S. are researchers of the Brazilian Council for Scientific and Technological Development (CNPq). We thank the LNLS technicians for their assistance. J.C.B. thanks FAPESP for the fellowship (Proc. No. 04/08966-2).

Appendix A. Supplementary data

Supplementary data associated with this article can be found, in the online version, at doi:10.1016/j.abb.2006.05.008.

References

[1] G.M. Davies, K.J. Barret-Bee, D.A. Jude, M. Lehan, W.W. Nichols, P.E. Pinder, J.L. Thain, W.J. Watkins, R.G. Wilson, Antimicrob. Agents Chemother. 38 (1994) 403 406.
[2] J.R. Coggins, in: A. Dodge (Ed.), Herbicides and Plant Metabolism, Cambridge University Press, Cambridge, UK, 1989, pp. 97 112.
[3] R. Bentley, Crit. Rev. Biochem. Mol. Biol. 25 (1990) 307 384.
[4] A.J. Pittard, in: F.C. Neidhardt, J.L. Ingraham, K.B. Low, B. Magasanik, M. Schaechter, H.E. Umbarger (Eds.), *Escherichia coli* and *Salmonella typhimurium*: Cellular and Molecular Biology, vol.1, American Society for Microbiology, Washington, DC, 1987, pp. 368 394.
[5] E. Haslam, Shikimic Acid: Metabolism and Metabolites, John Wiley, Chichester, United Kingdom, 1993.
[6] D. McDevitt, D.J. Payne, D.J. Holmes, M. Rosenberg, J. Appl. Microbiol. 92 (2002) 28S 34S.
[7] J.D. McArthur, N.P. West, J.N. Cole, H. Jungnitz, C.A. Guzman, J. Chin, P.R. Lehrbach, S.P. Djordjevic, M.J. Walker, FEMS Microbiol. Lett. 221 (2003) 7 16.
[8] M.F. Alibhai, W.C. Stallings, Proc. Natl. Acad. Sci. USA 98 (2001) 2944 2946.
[9] S. Eschenburg, W. Kabsch, M.L. Healy, E. Schönbrunn, J. Biol. Chem. 278 (2003) 49215 49222.
[10] H. Park, J.L. Hilsenbeck, H.J. Kim, W.A. Shuttleworth, Y.H. Park, J.N. Evans, C. Kang, Microbiology 51 (2004) 963 971.
[11] E. Schönbrunn, S. Eschenburg, W.A. Shuttleworth, J.V. Schloss, N. Amrhein, J.N. Evans, W. Kabsch, Proc. Natl. Acad. Sci. USA 98 (2001) 1376 1380.
[12] W.C. Stallings, S.S. Abdel-Meguid, L.W. Lim, H.S. Shieh, H.E. Dayringer, N.K. Leimgruber, R.A. Stegeman, K.S. Anderson, J.A. Sikorski, S.R. Padgette, G.M. Kishore, Proc. Natl. Acad. Sci. USA 88 (1991) 5046 5050.
[13] S. Eschenburg, M.L. Healy, M.A. Priestman, G.H. Lushington, E. Schönbrunn, Planta 216 (2002) 129 135.
[14] J.E. Ream, H.K. Yuen, R.B. Frazier, J.A. Sikorski, Biochemistry 31 (1992) 5528 5534.
[15] F. Krekel, C. Oecking, N. Amrhein, P. Macheroux, Biochemistry 38 (1999) 8864 8878.
[16] J.A. Sikorski, K.J. Gruys, Acc. Chem. Res. 30 (1997) 2 8.
[17] W. Du, W.S. Liu, D.J. Payne, M.L. Doyle, Biochemistry 39 (2000) 10140 10146.
[18] J.S. Oliveira, C.A. Pinto, L.A. Basso, D.S. Santos, Protein Expr. Purif. 22 (2001) 430 435.
[19] J.S. Oliveira, M.A. Mendes, M.S. Palma, L.A. Basso, D.S. Santos, Protein Expr. Purif. 28 (2003) 287 292.
[20] J.H. Pereira, F. Canduri, J.S. de Oliveira, N.J. da Silveira, L.A. Basso, M.S. Palma, W.F. De Azevedo Jr., D.S. Santos, Biochem. Biophys. Res. Commun. 312 (2003) 608 614.
[21] C.N. Pace, F. Vajdos, L. Fee, G. Grimsley, T. Gray, Protein Sci. 4 (1995) 2411 2423.
[22] J. García de la Torre, M.L. Huertas, B. Carrasco, Biophys. J. 78 (2000) 719 730.
[23] P. Schuck, Biophys. J. 78 (2000) 1606 1619.
[24] P. Schuck, M.A. Perugini, N.R. Gonzales, G.J. Howlett, D. Schubert, Biophys. J. 82 (2000) 1096 1111.
[25] T.M. Laue, Curr. Opin. Struct. Biol. 11 (2001) 579 583.
[26] G. Böhm, R. Muhr, R. Jaenicke, Protein Eng. 5 (1992) 191 195.
[27] O. Glatter, in: O. Glatter, O. Kratky (Eds.), Small Angle X-Ray Scattering, Academic Press, London, 1982.
[28] A. Guinier, G. Fournet, Small-Angle Scattering of X-rays, Wiley, New York, 1955.
[29] J.R. Olivieri, A.F. Craievich, Eur. Biophys. J. 24 (1995) 77 84.
[30] W.H. Press, S.A. Teukolsky, W.T. Vetterling, B.P. Flannery, Numerical Recipes in FORTRAN. The Art of Scientific Computing, second ed., Cambridge University Press, New York, 1992.
[31] W.F. De Azevedo, G.C. dos Santos, D.M. dos Santos, J.R. Olivieri, F. Canduri, R.G. Silva, L.A. Basso, G. Renard, I.O. da Fonseca, M.A. Mendes, M.S. Palma, D.S. Santos, Biochem. Biophys. Res. Commun. 309 (2003) 923 928.
[32] M.A. Priestman, T. Funke, I.M. Singh, S.S. Crupper, E. Schönbrunn, FEBS Lett. 579 (2005) 728 732.
[33] R.A. Laskowski et al., PROCHECK v.3.0 Program to Check the Stereochemistry Quality of Protein structures Operating Instructions (1994).
[34] D.I. Svergun, M.H.J. Koch, Rep. Prog. Phys. 66 (2003) 1735 1782.
[35] K.A. Brown, E.P. Carpenter, K.A. Watson, J.R. Coggins, A.R. Hawkins, M.H.J. Koch, D.I. Svergun, Bichem. Soc. T. 31 (2003) 543 547.
[36] H.C. Steinrücken, N. Amrhein, Eur. J. Biochem. 143 (1984) 351 357.
[37] R.S. Fischer, A. Berry, C.G. Gaines, R.A. Jensen, J. Bacteriol. 168 (1986) 1147 1154.
[38] W. Du, N.G. Wallis, M.J. Mazzulla, A.F. Chalker, L. Zhang, W.S. Liu, H. Kallender, D.J. Payne, Eur. J. Biochem. 267 (2000) 222 227.
[39] L.A. Basso, L.H. Pereira da Silva, A.G. Fett-Neto, W.F. de Azevedo Jr., I. de Souza Moreira, M.S. Palma, J.B. Calixto, S.A. Filho, R.R. dos Santos, M.B. Pereira Soares, D.S. Santos, Mem. Inst. Oswaldo Cruz. 100 (2005) 475 506.

5.2. Effects of the magnesium and chloride ions and shikimate on the structure of shikimate kinase from *Mycobacterium tuberculosis*. Acta Crystallogr Sect F Struct Biol Cryst Commun. 2007;63:1-6.

Acta Crystallographica Section F
Structural Biology and Crystallization Communications
ISSN 1744-3091

Effects of the magnesium and chloride ions and shikimate on the structure of shikimate kinase from *Mycobacterium tuberculosis*

Marcio Vinicius Bertacine Dias,[a] Lívia Maria Faím,[a] Igor Bordin Vasconcelos,[b] Jaim Simões de Oliveira,[b] Luiz Augusto Basso,[b] Diógenes Santiago Santos[b]* and Walter Filgueira de Azevedo Jr[c]*

[a]Programa de Pós-Graduação em Biofísica Molecular, Departamento de Física, UNESP, São José do Rio Preto, SP 15054-000, Brazil, [b]Pontifícia Universidade Católica do Rio Grande do Sul, Centro de Pesquisa em Biologia Molecular e Funcional, Porto Alegre, RS, Brazil, and [c]Faculdade de Biociências, Pontifícia Universidade Católica do Rio Grande do Sul, Av. Ipiranga, 6681 Porto Alegre-RS, CEP 90619-900, Brazil

Correspondence e-mail: diogenes@pucrs.br, walter.junior@pucrs.br

Received 27 September 2006
Accepted 6 November 2006

PDB References: shikimate kinase–ADP–shikimate complex, 2dfn, r2dfnsf; shikimate kinase–MgADP complex, 2dft, r2dftsf.

Bacteria, fungi and plants can convert carbohydrate and phosphoenolpyruvate into chorismate, which is the precursor of various aromatic compounds. The seven enzymes of the shikimate pathway are responsible for this conversion. Shikimate kinase (SK) is the fifth enzyme in this pathway and converts shikimate to shikimate-3-phosphate. In this work, the conformational changes that occur on binding of shikimate, magnesium and chloride ions to SK from *Mycobacterium tuberculosis* (MtSK) are described. It was observed that both ions and shikimate influence the conformation of residues of the active site of MtSK. Magnesium influences the conformation of the shikimate hydroxyl groups and the position of the side chains of some of the residues of the active site. Chloride seems to influence the affinity of ADP and its position in the active site and the opening length of the LID domain. Shikimate binding causes a closing of the LID domain and also seems to influence the crystallographic packing of SK. The results shown here could be useful for understanding the catalytic mechanism of SK and the role of ions in the activity of this protein.

1. Introduction

Mycobacterium tuberculosis, the aetiological agent of tuberculosis (TB), infects one-third of the world's population. It is estimated that 1.7 million deaths resulted from TB in 2004, 95% of which occurred in developing countries (World Health Organization, 2006). The emergence of TB as a public health threat, the high susceptibility of HIV/TB co-infected patients and the proliferation of multi-drug-resistant strains have created a need for newer and better drugs for the treatment of TB.

The shikimate pathway is an attractive target for the development of herbicides (Coggins, 1998) and antibiotic agents (Davies *et al.*, 1994) because it is essential in algae, higher plants, bacteria, fungi and apicomplexan parasites but is absent from mammals (Bentley, 1990; Roberts *et al.*, 1999). The shikimate pathway is a seven-step biosynthetic route that links the metabolism of carbohydrates to the synthesis of aromatic amino acids. The shikimate pathway leads to the biosynthesis of chorismate, which is a precursor of aromatic amino acids and many other aromatic compounds (Ratledge, 1982). Shikimate kinase (SK; EC 2.7.1.71), the fifth enzyme of this pathway, catalyzes phosphate transfer from ATP to the carbon-3-hydroxyl group of shikimate, forming shikimate 3-phosphate (S3P).

SK belongs to the nucleoside monophosphate (NMP) kinase structural family. SK is a α/β protein consisting of a central sheet of five parallel β-strands flanked by α-helices, with overall topology similar to that of adenylate kinase (Pereira *et al.*, 2004; Krell *et al.*, 1998, 2001). A characteristic feature of the NMP kinases is that they undergo large conformational changes during catalysis (Vonrhein *et al.*, 1995). The NMP kinases are composed of three domains: the CORE, which contains a highly conserved phosphate-binding loop (P-loop), the LID domain, which undergoes substantial conformational changes upon substrate binding, and the NMP-binding domain,

which is responsible for the recognition and binding of a specific substrate (Gu *et al.*, 2002).

MgADP induces concerted hinged movements of the shikimate-binding (SB) and LID domains such that the two domains move towards each other and towards the active centre of the enzyme in the presence of this ligand (Gu *et al.*, 2002).

The precise mode of binding of shikimate to MtSK and some conformational changes upon shikimate binding to MtSK have recently been proposed (Pereira *et al.*, 2004; Dhaliwal *et al.*, 2004). The binding of shikimate to MtSK causes a concerted conformational change of the LID and SB domains towards each other and results in an additional closure of the active site.

Chloride ions have been shown to weaken the interaction between shikimate and SK from *Erwinia chrysanthemi* and to strengthen the affinity of the enzyme for ADP and ATP (Cerasoli *et al.*, 2003). Thus, a chloride ion seems to occupy a site crucial for the binding of the nucleotide substrate in the correct orientation for catalysis.

In this work, we report two crystallographic structures: the MtSK–ADP–shikimate and MtSK–MgADP complexes. The MtSK–ADP–shikimate complex has been solved at 1.93 Å resolution. The crystal structure of MtSK in complex with ADP and Mg^{2+} has been solved at 2.8 Å resolution. The data presented here provide an evaluation of the effects of both Mg^{2+} and Cl^- ions and shikimate on the structure of MtSK. Thus, these results provide further insight into the roles that different ions and substrate play in the mechanism of action of MtSK.

2. Materials and methods

2.1. Crystallization

The cloning, expression and purification of MtSK have been reported elsewhere (Oliveira *et al.*, 2001). Initially, MtSK was concentrated to 14 mg ml^{-1} and dialyzed against 50 m*M* Tris–HCl buffer pH 8.0. For the crystallization of MtSK in complex with ADP and shikimate in the absence of Mg^{2+} ion, variations of the crystallization condition established by Dhaliwal *et al.* (2004) were used. Crystals were obtained by the hanging-drop vapour-diffusion method. The well solution contained 0.1 *M* Tris–HCl buffer pH 8.0, 17% PEG 1500 and 0.5–0.7 *M* LiCl. The drops had a protein solution:well solution volume ratio of 1.6:1.0. For the crystallization of the protein in complex with ADP and Mg^{2+} in the absence of shikimate, a crystallization solution composed of 0.1 *M* Tris–HCl buffer pH 8.0, 20% PEG 3350 and 0.1 *M* $MgCl_2.6H_2O$ was used. The concentration of the protein was 17 mg ml^{-1} and the drops again had a protein solution:well solution volume ratio of 1.6:1.0.

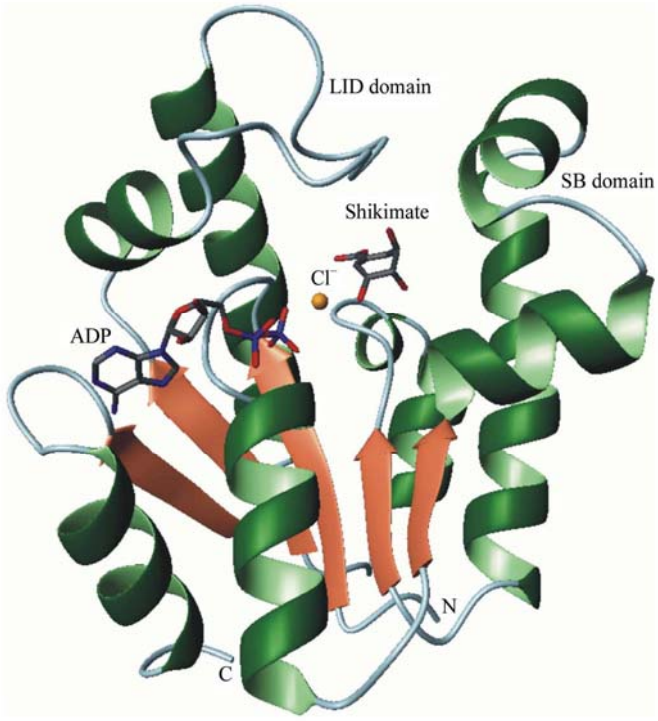

(*a*)

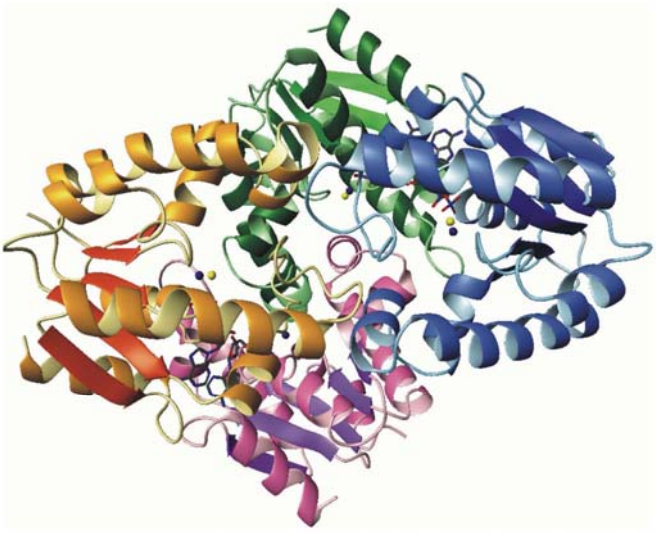

(*b*)

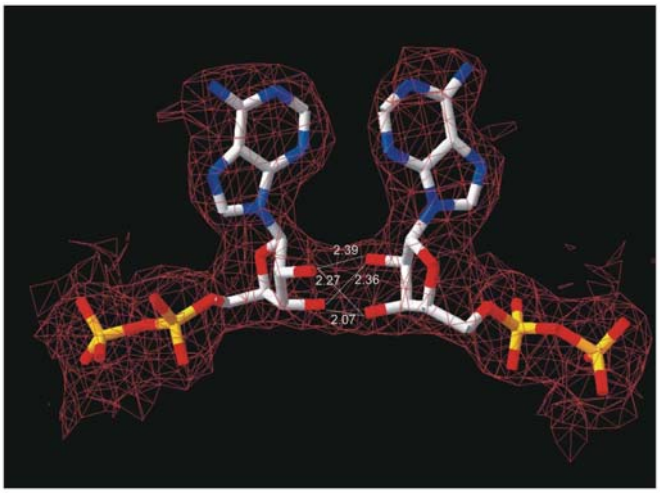

(*c*)

Figure 1
(*a*) Structure of MtSK in complex with ADP, shikimate and Cl^-. (*b*) Tetrameric structure of MtSK in complex with ADP, Mg^{2+} and Cl^-. The monomers *A*, *B*, *C* and *D* are represented in green, blue, pink and yellow, respectively. The dark blue and yellow spheres represent the magnesium and chloride ions, respectively. The ADP molecules are represented as sticks. (*c*) Representation of the hydrogen-bonding interactions that occur between the ribose hydroxyl groups of ADP molecules bound to monomers *A* and *B*. The distances are shown in Å. Figures were generated with the program *MolMol* (Koradi *et al.*, 1996).

2.2. Data collection and processing

All data sets were collected at a wavelength of 1.427 Å using a synchrotron-radiation source (Station PCr, LNLS, Campinas, Brazil; Polikarpov *et al.*, 1998) and a CCD detector (MAR CCD). Data collection was performed under cryogenic conditions at a temperature of 100 K in a cold nitrogen stream generated and maintained with an Oxford Cryosystem. Prior to flash-cooling, glycerol was added to the crystallization drop to 20%(*v*/*v*). The data sets were processed using the program *MOSFLM* (Leslie, 1992) and scaled with *SCALA* (Collaborative Computational Project, Number 4, 1994).

2.3. Structure determination

The crystal structures of both complexes were determined by standard molecular-replacement methods using the program *AMoRe* (Navaza, 2001). For both complexes, we used as a search model the structure of MtSK–MgADP–shikimate (PDB code 1we2; Pereira *et al.*, 2004). Refinement of the structures was performed using *REFMAC*5 implemented in the *CCP*4 package (Murshudov *et al.*, 1997; Collaborative Computational Project, Number 4, 1994). *Xtal-View*/*Xfit* (McRee, 1999) was used for visual inspection and addition of water molecules. The stereochemical correctness of the models was checked using *PROCHECK* (Laskowski *et al.*, 1993). The final atomic models were superposed using *LSQKAB* from the *CCP*4 package (Collaborative Computational Project, Number 4, 1994). *PARMODEL* (Uchôa *et al.*, 2004) was used in the final analysis of the model.

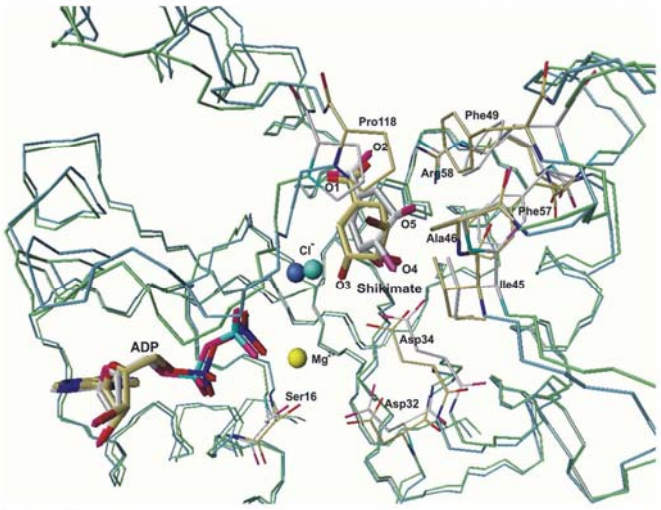

Figure 2
Superposition of the structures of the MtSK–MgADP–shikimate and MtSK–ADP–shikimate ternary complexes. The C^{α} trace of the MtSK–MgADP–shikimate complex is presented in green and that of the MtSK–ADP–shikimate trace is presented in blue. The C atoms of MtSK–MgADP–shikimate and MtSK–ADP–shikimate are coloured white and yellow, respectively. The Mg^{2+} shown in yellow and the chloride ion shown in turquoise refer to the MtSK–MgADP–shikimate structure, while the chloride ion in dark blue refers to the MtSK–ADP–shikimate structure. The figure was generated with the program *MolMol* (Koradi *et al.*, 1996).

3. Results and discussion

MtSK crystallized in two different space groups depending on the complex. The crystals of the MtSK–ADP–shikimate ternary complex were trigonal, space group $P3_221$, and diffracted to 1.93 Å resolution. The asymmetric unit contains one molecule and the final values of R and $R_{\rm free}$ were 20.2 and 27.0%, respectively. In contrast, the crystals of the MtSK–ADP–Mg^{2+} ternary complex were orthorhombic, space group $P2_12_12_1$, and diffracted to 2.8 Å resolution. The asymmetric unit contains four MtSK monomers that form a tetramer and the final values of R and $R_{\rm free}$ were 18.3 and 28.0%, respectively. Table 1 details the data processing, refinement statistics and quality analysis of the two complexes.

The structures present good geometry, although some residues of the LID domain are located in disallowed regions of the Ramachandran plot. The N-terminal methionine residue is not observed since it was removed during the MtSK expression in *E. coli* (Oliveira *et al.*, 2001). The ten C-terminal residues are disordered in both structures and have not been included in the final structure.

The folding of the MtSK complexes presented here is similar to that of those reported previously (Pereira *et al.*, 2004; Krell *et al.*, 1998; Gu *et al.*, 2002; Dhaliwal *et al.*, 2004). SK is a α/β protein and consists of five central parallel β-strands flanked by α-helices. Fig. 1(*a*) shows a ribbon representation of the secondary-structure elements of MtSK–ADP–shikimate at 1.93 Å resolution.

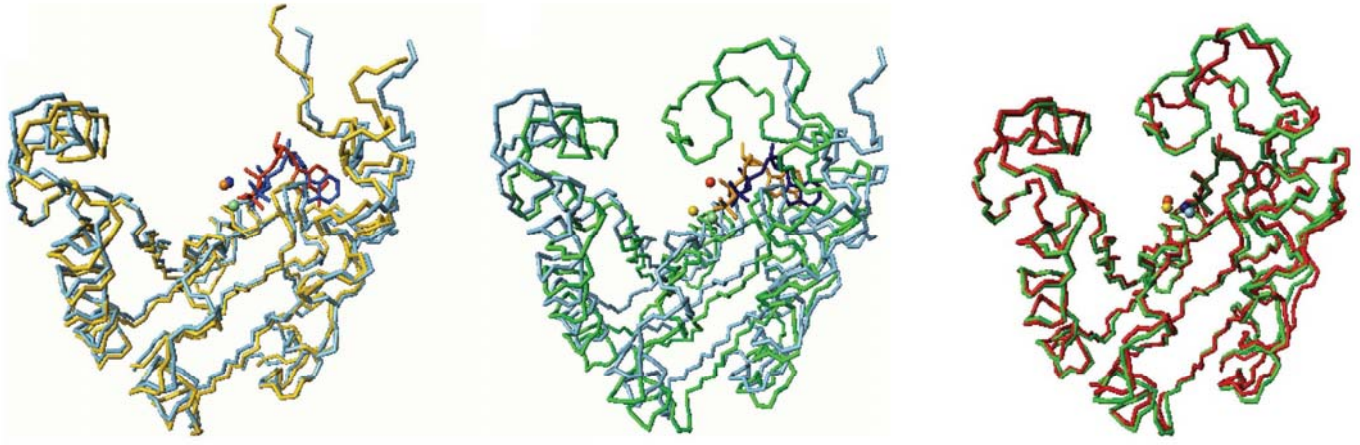

Figure 3
Superposition of the chains of the structure of the MtSK–MgADP binary complex obtained in the absence of shikimate. (*a*) Chains *A* (yellow) and *C* (light blue), (*b*) chains *B* (green) and *C* (light blue) and (*c*) chains *B* (green) and *D* (red).

3.1. Structure of the MtSK–ADP–Mg^{2+} ternary complex

The asymmetric unit of the MtSK–ADP–Mg^{2+} ternary complex structure contains four monomers forming a homotetramer with 222 symmetry. However, each subunit presents a different conformation state. In the *A* and *C* subunits the LID domain is disordered and residues 115–123 and 114–123 were thus not included in the final model.

The structure of the MtSK tetramer is shown in Fig. 1(*b*). Each monomer is in contact with the other three, creating an intricate packing arrangement. The ADP molecules appear to play an important role in the stabilization of the tetramer, since the hydroxyl groups of the ribose moiety of ADP of one monomer form hydrogen bonds with those of a neighbouring monomer (Fig. 1*c*).

3.2. Influence of Mg^{2+} on the structure of MtSK

The absence of Mg^{2+} ions seems to have a significant effect on the position of shikimate and some of the active-site residues, mainly Asp32 and Asp34 (these are conserved residues in all SKs and are involved in the binding of Mg^{2+}; Fig. 2). In addition, the chloride ion and ADP molecule also undergo changes in position. Fig. 2 shows a superposition of the MtSK–MgADP–shikimate (Pereira *et al.*, 2004) and MtSK–ADP–shikimate complexes, showing the structural changes caused by the absence of the Mg^{2+} ion.

In the structure of the MtSK–ADP–shikimate ternary complex, the 3-, 4- and 5-hydroxyl groups of shikimate undergo a shift in their positions, leading to small differences in the hydrogen-bonding pattern between shikimate and MtSK. Although the Asp34 residue interacts with shikimate in both structures, a hydrogen bond between the OD2 atom of Asp34 and the O3 atom of the shikimate is not observed in the MtSK structure without Mg^{2+} (not shown).

The position of the chloride ion is closer to shikimate in the MtSK–ADP–shikimate ternary complex than in the MtSK–MgADP–shikimate complex (Pereira *et al.*, 2004). In the structure of the MtSK–ADP–shikimate ternary complex, the chloride ion is 2.4 Å away from the O1 atom of the shikimate 3-hydroxyl group, while in the structure of MtSK–MgADP–shikimate the distance between these two atoms is 3.4 Å. The absence of the Mg^{2+} ion can also cause alterations in the side chains of the hydrophobic residues Phe49 and Phe57 located in the SB domain and of Pro118, Ala46 and Ile45 located in the LID domain (Fig. 2).

As established previously for other NMP kinases, the Mg^{2+} ion is expected to play an important role in the transfer of the γ-phosphate group of ATP to the nucleophilic 3-OH group of shikimate by an associative reaction mechanism (Schlichting & Reinstein, 1997; Bellinzoni *et al.*, 2006). Thus, the differences observed in the MtSK–ADP–shikimate ternary complex in the absence of Mg^{2+} may contribute to understanding of the MtSK chemical mechanism.

3.3. Influence of chloride ion on the structure of MtSK

In our structure of the MtSK–MgADP binary complex, monomer *C* of the MtSK tetramer does not contain chloride ion. This ion seems to influence the position of the ADP molecule and the position of the shikimate molecule. This monomer presents a conformation that is more open than the other monomers (Fig. 3). Furthermore, the LID domain of monomer *C* has a mean *B* factor that is higher than those of the other monomers (not shown). The ADP molecule bound to monomer *C* is shifted by approximately 3.0 Å in the active site (Fig. 3) compared with the other monomers of the MtSK tetramer or with other structures of MtSK in complex with ADP. These results are in

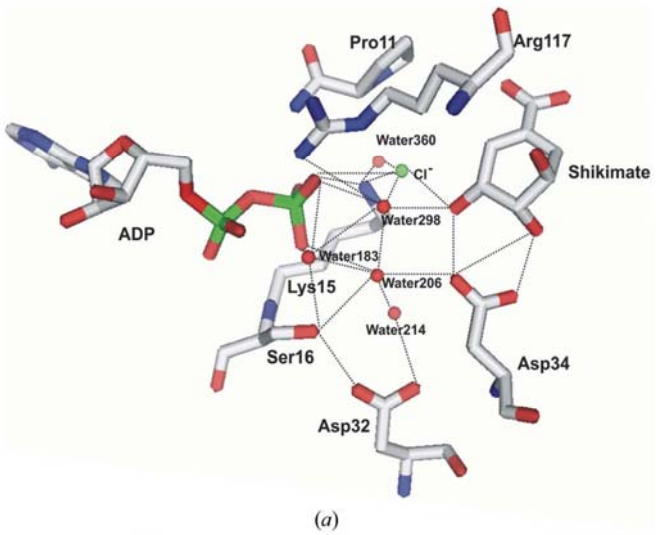

(*a*)

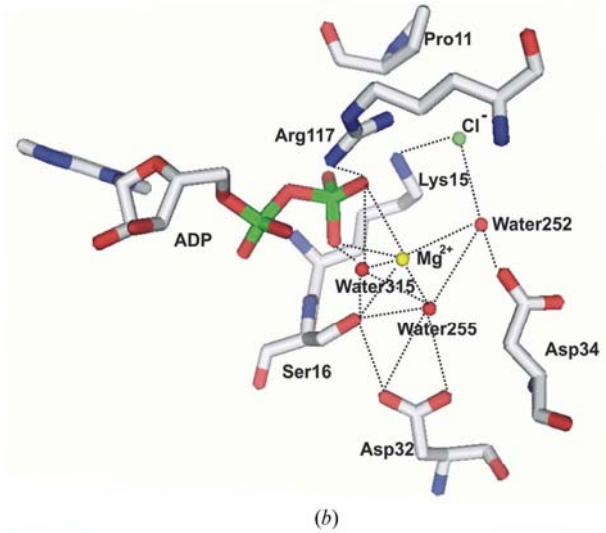

(*b*)

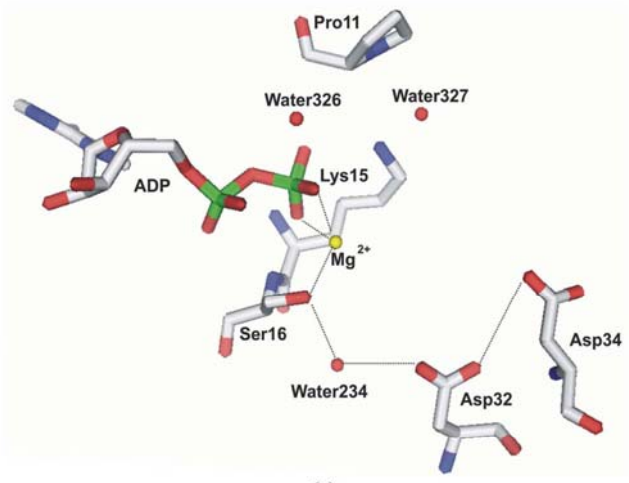

(*c*)

Figure 4
Pattern of water bonding in the active site of MtSK. (*a*) Structure at 1.93 Å resolution (chloride ion and shikimate present, magnesium ion absent), (*b*) monomer *B* of the tetramer (chloride and magnesium ions present, shikimate absent), (*c*) monomer *C* of the tetramer (magnesium ion present, shikimate and chloride ion absent). The figures were generated using *PyMOL* (DeLano, 2004).

Table 1
Crystallographic data, refinement statistics and analysis of the quality of MtSK structures.

Values in parentheses are for the outermost shell.

	MtSK–ADP–shikimate	MtSK–MgADP
Crystallographic data		
Unit-cell parameters		
a (Å)	63.3	60.2
b (Å)	63.3	62.2
c (Å)	91.6	170.6
Space group	$P3_221$	$P2_12_12_1$
No. of measurements	76792	97059
No. of independent reflections	16017	17057
Completeness (%)	96.9 (91.5)	99.4 (96.9)
R_{sym}† (%)	8.9 (58.8)	12.1 (58.0)
Redundancy	4.8	5.7
Refinement statistics		
Resolution range (Å)	35.16–1.93	57.17–2.80
Reflections used for refinement	15130	15670
Final *R* factor‡ (%)	20.2	18.3
Final R_{free}§ (%)	27.0	28.0
Correlation coefficient (%)	95.2	94.3
B values (Å^2)		
Main chain	31	33
Side chain	34	36
ADP	21	27
Shikimate	32	—
Waters	39	30
Quality of structure		
Three-dimensional profile¶	S = 88.07, IS = 74.95, S/IS = 1.18IS	S = 343.59, IS = 294.34, S/IS = 1.17IS
Ramachandran plot		
Favoured	95.6	84.8
Additionally allowed	2.9	13.3
Generously allowed	0.7	0.8
Disallowed	0.7	1.1

† $R_{sym} = 100\sum I(h) - \langle I(h)\rangle|/\sum I(h)$, where $I(h)$ is the observed intensity and $\langle I(h)\rangle$ is the mean intensity of reflection h over all measurements of $I(h)$. ‡ R factor $= 100\sum |F_{obs} - F_{calc}|/\sum F_{obs}$, the sums being taken over all reflections with $F/\sigma(F) > 2\sigma(F)$. § R_{free} is the R factor for 10% of the data that were not included during crystallographic refinement. ¶ The ideal score measures the compatibility of a protein model with its sequence, using a 3D profile. Each residue position in the 3D model is characterized by its environment and is represented by a row of 20 numbers in the profile. These numbers are the statistical preferences (called 3D-1D scores) of each of the 20 amino acids for this environment. Environments of residues are defined by three parameters: the area of the residue that is buried; the fraction of side chain area that is covered by polar atoms (O and N) and the local secondary structure. The 3D profile score *S* for the compatibility of the sequence with the model is the sum, over all residue positions, of the 3D-1D scores for the amino-acid sequence of the protein. For 3D protein models known to be correct, the 3D profile score S for the amino-acid sequence of the model is high, by contrast, the profile score S for the compatibility of a wrong 3D protein model with its sequence is often low. When this method is used to verify a structure, the raw compatibility score alone is difficult to interpret. In this case it is necessary to compare the score to those obtained using structures known to be correct, we use the Ideal Score (IS), that is calculated from the length of the protein. The IS is determined by $IS = \exp[-0.83 + 1.008 \times \ln(L)]$. Where L is the length of the sequence. Severely misfolded structures typically have scores less than 0.45 IS. A score near or above IS indicates a reliable structure.

agreement with the kinetic and spectroscopic data previously obtained by Cerasoli *et al.* (2003). This work shows that the chloride ion increases the stability of the *E. chrysanthemi* SK structure and that this same ion also influences the affinity of ADP for SK. Thus, the increase in the protein stability may be a consequence of chloride favouring the SK structure in its closed state.

The chloride ion bound to the MtSK active site seems to be part of an intricate network formed of water molecules, residues of the LID and SB domains, ADP and shikimate. This network of interactions appears to cause closure of the structure (Fig. 4). In all structures of MtSK reported so far and in the three monomers of the MtSK tetramer, an interaction network involving three water molecules is formed in the active site (Fig. 4). These water molecules bridge the interactions between ADP, chloride and magnesium ion and MtSK. In our MtSK–ADP–shikimate ternary complex, water 306 occupies a similar position to the Mg^{2+} ion. In the absence of chloride ion, this phenomenon does not occur and furthermore the formation of this intricate network that can induce the opening of the structure is avoided.

3.4. Influence of shikimate in the structure of MtSK

The crystals of the MtSK–MgADP binary complex in the absence of shikimate were obtained in space group $P2_12_12_1$, which has not been previously described for MtSK. The asymmetric unit presents four MtSK monomers that form a tetramer. The absence of shikimate from the crystallization conditions influences the crystal packing and also the conformation of the SB and LID domains of MtSK, as observed by Pereira *et al.* (2004) and Dhaliwal *et al.* (2004). In accordance with this, Gan and coworkers recently solved the apo-MtSK and MtSK–shikimate binary complex structures and suggested that shikimate binding defines the conformational change of the protein that arises when shikimate is bound: the LID domain is ordered and closes over the bound shikimate (Gan *et al.*, 2006).

4. Conclusion

Here, we report two structures of shikimate kinase from *M. tuberculosis*: the MtSK–ADP–shikimate and MtSK–MgADP complexes. In the former, we observe the effect of the Mg^{2+} ion on the structure and in the latter we observe the effect of shikimate on the crystal packing and on the structure of MtSK. The Mg^{2+} ion seems to influence the position of the hydroxyl groups of the shikimate molecule and some of the residues of the active site of MtSK. The crystal structure of the MtSK–MgADP complex was solved in space group $P2_12_12_1$, which has not previously been described for MtSK. In this space group, the MtSK presents a tetramer with 222 symmetry, in which the ribose moiety of the ADP molecule seems to play an important role in the stabilization of the tetramer and the contacts between the monomers, which occur mainly in the LID-domain region. However, one monomer of the tetramer does not contain chloride ion. The absence of this ion seems to cause large changes in the position of the ADP molecule and also causes a large opening of MtSK. This information is accordance with the results obtained by Cerasoli *et al.* (2003), which shows the importance of the chloride ion in the stability and the alignment of the substrates in the active site of SK.

We hope that the results described here will shed light on the structural changes of MtSK upon binding of substrate(s) that will be useful for the understanding of the catalytic mechanism and for structure-based drug design of novel inhibitors that may be potential anti-mycobacterial agents.

This work was supported by grants from FAPESP (SMOLBNet, Proc. 01/07532-0, 03/12472-2, 04/00217-0), CNPq, CAPES and Instituto do Milênio (CNPq-MCT), DSS, WFA (CNPq, 300851/98-7) and LAB (CNPq, 520182/99-5) are researchers of the Brazilian Council for Scientific and Technological Development.

References

Bellinzoni, M., Haouz, A., Grana, M., Munier-Lehmann, H., Shepard, W. & Alzari, P. M. (2006). *Proteins*, **15**, 1–5.
Bentley, R. (1990). *Crit. Rev. Biochem. Mol. Biol.* **25**, 307–384.
Cerasoli, E., Kelly, S. M., Coggins, J. R., Lapthorn, A. J., Clarke, D. T. & Price, N. C. (2003). *Biochim. Biophys. Acta*, **1648**, 43–54.
Coggins, J. R. (1998). In *Herbicides and Plant Metabolism*, edited by A. Dodge. Cambridge University Press.

Collaborative Computational Project, Number 4 (1994). *Acta Cryst.* D**50**, 760–763.
Davies, G. M., Barret-Bee, K. J., Jude, D. A., Lehan, M., Nichols, W. W. & Pinder, P. E. (1994). *Agents Chemother.* **38**, 403–406.
DeLano, W. L. (2004). *The PyMOL Molecular Graphics System.* DeLano Scientific, San Carlos, CA, USA.
Dhaliwal, B., Nichols, C. E., Ren, J., Lockyer, M., Charles, I., Hawhins, A. R. & Stammers, D. K. (2004). *FEBS Lett.* **574**, 49–54.
Gan, J., Gu, Y., Li, Y., Yan, H. & Ji, X. (2006). *Biochemistry*, **45**, 8539–8545.
Gu, Y., Reshetnikova, L., Li, Y., Wu, Y., Yan, H., Singh, S. & Ji, S. (2002). *J. Mol. Biol.* **319**, 779–789.
Koradi, R., Billeter, M. & Wüthrich, K. (1996). *J. Mol. Graph.* **14**, 51–55.
Krell, T., Coggins, J. R. & Lapthorn, A. J. (1998). *J. Mol. Biol.* **278**, 983–997.
Krell, T., Maclean, J., Boam, D. J., Cooper, A., Resmini, M., Brocklehurst, K., Kelly, S. M., Price, N. C., Lapthorn, A. J. & Coggins, J. (2001). *Protein Sci.* **10**, 1137–1149.
Laskowski, R. A., MacArthur, M., Moss, D. S. & Thornton, J. M. (1993). *J. Appl. Cryst.* **26**, 283–291.
Leslie, A. G. W. (1992). *Jnt CCP4/ESF–EACBM Newsl. Protein Crystallogr.* **26**.
McRee, D. E. (1999). *J. Struct. Biol.* **125**, 156–165.
Murshudov, G. N., Vagin, A. A. & Dodson, E. J. (1997). *Acta Cryst.* D**53**, 240–255.
Navaza, J. (2001). *Acta Cryst.* D**57**, 1367–1372.
Oliveira, J. S., Pinto, C. A., Basso, L. A. & Santos, D. S. (2001). *Protein Expr. Purif.* **22**, 430–435.
Pereira, J. H., Oliveira, J. S., Canduri, F., Dias, M. V. B., Palma, M. S., Basso, L. A., Santos, D. S. & Azevedo, W. F. Jr (2004). *Acta Cryst.* D**60**, 2310–2319.
Polikarpov, I., Perles, L. A., de Oliveira, R. T., Oliva, G., Castellano, E. E., Garratt, R. C. & Craievich, A. (1998). *Nucl. Instrum. Methods Phys. Res. A*, **405**, 159–164.
Ratledge, C. (1982). *The Biology of the Mycobacteria*, Vol. 1, edited by C. Ratledge & J. L. Stanford, pp. 185–271. London: Academic Press.
Roberts, F., Roberts, C. W., Johnson, J. J., Kyle, D. E., Krell, T., Coggins, G. H., Milhous, W. K., Tzipoki, S., Ferguson, D. J., Chakrabarti, D. & McLeod, R. (1999). *Nature (London)*, **397**, 219–220.
Schlichting, I. & Reinstein, J. (1997). *Biochemistry*, **36**, 9290–9296.
Uchôa, H. B., Jorge, G. E., Silveira, N. J. F., Câmera, J. C., Canduri, F. & Azevedo, W. F. Jr (2004). *Biochem. Biophys. Res. Commun.* **325**, 1481–1486.
Vonrhein, C., Schlauderer, G. J. & Schulz, G. F. (1995). *Structure*, **3**, 483–490.
World Health Organization (2006). *Tuberculosis – Fact Sheet No.* 104. http://www.who.int/mediacentre/factsheets.